

IBM Research Report

Characterization and Performance Evaluation of Differential Shielded Cables for Multi-Gb/s Data-rates

**Alina Deutsch, Gerard V. Kopcsay, Christopher W. Surovic,
Paul W. Coteus, Alphonso P. Lanzetta, Todd Takken,**

IBM Research Division
Thomas J. Watson Research Center
P.O. Box 218
Yorktown Heights, NY 10598

P. W. Bond
IBM Development Laboratory,
2455 South Road, Poughkeepsie, NY 12601



Research Division
Almaden - Austin - Beijing - Delhi - Haifa - India - T. J. Watson - Tokyo - Zurich

Characterization and Performance Evaluation of Differential Shielded Cables for Multi-Gb/s Data-rates

A. Deutsch, G. V. Kopcsay, C. W. Surovic, P. W. Coteus, A. P. Lanzetta, T. Takken, P. W. Bond¹

IBM Research Division, Thomas J. Watson Research Center, P. O. Box 218, Yorktown Heights, NY 10598
email: deutsch@us.ibm.com, Phone: (914) 945-2858; Fax: (914) 945-2141

¹IBM S/390 Development Laboratory, 2455 South Road, Poughkeepsie, NY 12601

Abstract This paper compares several differential cable characteristics that were evaluated for multi-Gb/s data-rates for both data and clock paths for 1 – 10 m lengths. Time-domain measurements are shown for the unassembled and connectorized cables and for representative card-plus-cable signal paths and the performance limiting factors are highlighted. Techniques are shown for developing coupled-line models for odd and even excitations for all the components in a full chip-to-chip path in order to make realistic data-rate predictions.

Keywords – *Lossy transmission-lines, shielded cables, differential time-domain measurements and simulations, measurement and modeling of skin-effect and dielectric losses on printed-circuit-board wiring and cables, data-rate and bandwidth.*

Introduction

The rapid increase in available microprocessor clock rates that approach 3.5 GHz today [1], is placing higher demands on the performance of the chip-to-chip interconnections. Such paths are still lagging behind with at most 300 – 500 MHz rates. Digital computing complexes, the Internet infrastructure, and massively parallel, supercomputers and distributed machines are demanding higher bandwidth and density for these interconnections. This is driven by the need for higher data bandwidth in order to support these faster processors, I/O's, memory subsystems, and second, because of the need for more system concurrency. A couple of standards are emerging today, such as RapidIO [2] and Infiniband [3] for intra-system and system-area-networks (SAN) that promise data rates of 2.5 – 10 Gb/s. Communication packet switches and network processors require 1 Tb/s aggregate bandwidth already [4, 5].

A typical data or clock path will start from the driver circuit on a chip mounted on a chip-carrier that is attached to a card, connected to a board, and then arrives at the receiver circuit on another chip attached to another card. Depending on the system architecture and size, the board wiring can be replaced by longer cables. Point-to-point, terminated, differential signaling has been increasingly used with the higher data rates and wider buses. It offers improved noise margin due to reduction in simultaneously-switching noise on wide buses and reflection noise from package discontinuities, higher immunity to externally generated noise and lower EMI (electro-magnetic interference or radiation). Because of the canceling effect of the odd-mode, + -, excitation, the effect of reflections from connectors, vias, wire-bonds, flip-chip solder balls, redistribution leads, poorly referenced transmission-lines is greatly reduced, resulting in lower signal distortion and thus higher performance.

In this paper, we show a methodology for detailed analysis of several shielded differential cables. The study includes measurements of the unassembled cables, of the cables with attached connectors, and the cables as part of a representative signal path with card wiring included. Coupled-line models for odd and even mode excitations are developed for the cables and card wiring based on the experimentally extracted electrical parameters. The entire study relies on time-domain measurements. The results were found to be very similar to network-analyzer-based frequency domain measurements that are traditionally used by cable suppliers. Signal propagation measurements are compared to simulated results for representative lengths and pulse widths of 334 ps to 1.19 ns. The developed models are thus validated and used to evaluate the relative performance of the various cable options. The study focuses on cables without any circuit or cable compensation and thus highlights the limited data-rates and lengths that uncompensated cables can achieve.

I. Unassembled Cable Analysis

Three types of cables were analyzed that are representative for the type of data rates and lengths in use today and in the near future, namely 1 – 10 Gb/s and 1 – 10 m lengths. The cross sections are shown in Figs. 1, 2 and 3. Fig. 1 shows an AWG26 differential cable [6] that is very similar to the type of cables planned for the Infiniband interconnections. This cable has two, 16.4-mil-diameter signal conductors, one ground drain conductor, with 13-mil-diameter (AWG28) and a thin foil shield wrapped around the assembly that is 0.63-mil-thick. The effective dielectric constant of the Teflon insulator is $\epsilon_r = 1.65$. The outer dimensions are 60x100 mils. Fig. 2 shows the AWG24 differential cables manufactured with stranded signal and outer braided shield for the ground return [7]. The insulator dielectric that is wrapped Teflon results in $\epsilon_r = 1.3$. The signal conductors are made out of seven 6.8-mil-diameter conductors while the braided shield uses 4.2-mil-diameter conductors. There is also a 0.67-mil thick foil wrapped underneath the braid. Overall thickness of braid is about 20.3 mils. The two signal lines have a center-to-center separation of 40.4 mils with an average diameter of 20 mils. The outer dimensions are 90x125 mils. Finally, Fig. 3 shows the cross section for the RG400 coaxial cables used as two, phase-matched pairs. These cables use 38.6-mil signal conductor diameter made out of 19 strands of 8.5-mil-diameter conductors. The braided-shield has 5.7-mil-diameter wires with a total thickness of 25.4 mils. The inner dielectric material diameter is 116 mils, and there is an outer coating above the shield of 22.4 mils. The overall outer diameter is 211 mils. All conductors are copper with 1-*mm* -thick tin coating. In this case, the Teflon dielectric constant is $\epsilon_r = 2.0$.

In all cases, the unassembled cables, without the end connectors were characterized first. This allowed us to extract all the necessary parameters to generate an accurate model for the cables without the discontinuities generated by the cable connectors and the interface to the card wiring. Fig. 4 shows the test arrangement we used for the AWG26 and AWG24 cables and Fig. 5 shows the layout of the card test pads used. The cable ends are soldered to small test pads that allow testing with coaxial probes. Such configurations introduce minimal end discontinuities compared to traditional measurement practice where test card traces connect through SMA connectors to the test equipment. The coaxial probes [8] that were used, with one signal and one ground tip, were characterized with the use of a 70 GHz sampling oscilloscope [9] and found to be able to transmit 12-ps rise-times or having an equivalent bandwidth of 29 GHz, that is quite adequate for 1 – 10 GHz signaling.

The test pads also allow for four-point resistance and signal line capacitance measurements. Sections of cables are also cross-sectioned to obtain the actual dimensions. As can be noticed in Figs. 1-3, there could be significant non-uniformity along the length. The AWG26 cables could have the drain wire shift from the ideal central position and thus create an imbalance in the differential characteristics. The AWG24 cables have irregular dielectric cross section due to the softer insulator used in order to reduce the dielectric constant and the thinner layer used due to the lower ϵ_r . The RG400 cable has less non-uniformity, other than caused by the use of stranded signal and shield, but it is also a much stiffer and bulkier construction that results in more cumbersome use.

a. Resistance

In the case of the AWG26 cables, the solid signal conductors had $R = 0.00135 \Omega/\text{cm}$ and the ground return had $R_{\text{GND}} = 0.00161 \Omega/\text{cm}$. Based on these values and the cross sectional dimensions obtained, the copper resistivity for the signal conductors was extracted to be $r = 1.837 \mu\Omega\text{cm}$. The shield is made of aluminum with $r = 2.64 \mu\Omega\text{cm}$. In the case of the AWG24 cable, the resistance is reduced by only 7.7 %, to $R = 0.001244 \Omega/\text{cm}$, even though the difference in diameter is 23.8%. This small difference in resistance is caused by the use of stranded conductors for larger diameter cables in order to maintain flexibility. The R_{GND} in this case is $R_{\text{GND}} = 0.000227 \Omega/\text{cm}$. The RG400 cables have $R = 0.00029 \Omega/\text{cm}$ and $R_{\text{GND}} = 0.00008833 \Omega/\text{cm}$.

b. Capacitance

Line capacitance was measured at 1 MHz and resulted in self capacitance $C_{11} = C_{22} = 0.827 \text{ pF}/\text{cm}$, and mutual capacitance $C_{12} = 0.031 \text{ pF}/\text{cm}$ for the AWG26 cables. The calculated values agreed very well, namely $C_{11} = C_{22} =$

0.82766 pF/cm and $C_{12} = 0.03118$ pF/cm. Measurements are usually made for two lengths of lines and the difference is taken between the results and divided by the difference in lengths. This then eliminates the errors introduced by the parasitic capacitance of end pads and probes. For the AWG24 cables, $C_{11} = C_{22} = 0.7206$ pF/cm and $C_{12} = 0.0658$ pF/cm. The resultant odd-mode excitation, + -, capacitance, is $C_{\text{odd}} = C_{11} + C_{22} = 0.8588$ pF/cm for AWG26 and 0.7864 pF/cm for the AWG24 cables. The 8.4% difference is due to the lower dielectric constant used of 1.3 vs. 1.65. For the RG400 cables, $C = 1.018$ pF/cm. These cables have the highest ϵ_r of 2.0. Since most of these interconnections are used for serial data packet transmission or system architectures where latency penalty is not significant, the difference in dielectric constant and therefore in delay, is not a deciding factor in cable selection.

c. Characteristic Impedance

TDR (time-domain-reflection) measurements were performed using 30-ps step excitation from a 20-GHz Tektronix 11801 sampling oscilloscope with two SD-24 sampling heads. Due to the differential use, four coaxial probes, two input, and two output, are needed as shown in Fig. 4. The measurement is performed in either odd-mode, + -, or even-mode, + +, with each signal conductor receiving either a positive going or a negative going step signal. The referencing of all the four probes is to the return ground provided either by the drain wire, or braided shield. This arrangement is equivalent to using a differential probe across the two signal conductors. The two sources and the two scope detectors have to be synchronized very carefully in spite of physical unevenness and scope timing drift. Moreover, the two cables, even in a differential configuration, exhibit unevenness, as seen in Fig. 6. In an odd-mode excitation case, the imbalances will cancel out at the detector end while in the even-mode, + +, the signal return is through the lossy, irregular shield or drain wire. The TDR even-mode trace in Fig. 6 shows all the cable irregularity along the length.

II. Frequency Dependent Losses

The short-pulse propagation technique described in [10] was used to extract the attenuation, characteristic impedance, and phase constant as a function of frequency. Because of the large diameter of the copper conductors used in these cables, skin-effect induced resistive losses become significant at very low frequencies. In such structures, skin-depth, \mathbf{d} , [11] is much smaller than the conductor diameter, \mathbf{f} , or $\mathbf{d} \ll \mathbf{f}$. On the other hand, 2.5 Gb/s – 10 Gb/s data-rate signals have rise-times with a fairly broad frequency spectrum greater than 10 GHz. The Teflon insulators have very small dielectric loss, however, the additional losses this generates can limit the maximum useable cable length. Skin-effect induced losses increase in proportion to \sqrt{f} , where f is the frequency, while dielectric loss increases in proportion to f , since conductance $G = \mathbf{w}Ct\mathbf{and}$, where $\mathbf{w} = 2\mathbf{p}f$ (attenuation is proportional to G , [11]). Both losses are then important due to the very long lengths and fast rise times required [12]. Moreover, some of the cables have tinned copper (Fig. 3), aluminum drain wire (Fig. 1), stranded cross section (Figs. 2 and 3) and irregular braid cross section (Figs. 2 and 3). Additional losses are generated by these effects that have to be accounted for.

The short-pulse propagation technique [10] directly measures $\mathbf{b}(f)$, $\mathbf{a}(f)$, and $Z_o(f)$ over a broad frequency range even though it is performed in the time domain using the same sampling oscilloscope used for TDR and TDT (time-domain-transmission) measurements. Two short electrical pulses, + -, or + +, are launched onto the cables and the transmitted waveforms are recorded at the output end. These pulses are 30-ps wide and can easily be obtained by differentiating the two step sources from the sampling oscilloscope. Two passive, impulse forming networks (Picosecond Pulse Labs model 5208) can be used as the differentiators. Fig. 7 shows the propagated pulses on 1-m- and 3-m-long AWG24 cables. These pulses are digitized and numerically Fourier transformed. Time windowing is used to eliminate any unwanted end reflections and therefore the Fourier spectra contain information about the forward traveling waves only. The ratio of complex spectra then yields the propagation constant

$$\Gamma(f) = \mathbf{a}(f) + j\mathbf{b}(f) = \frac{1}{l_1 - l_2} \ln \frac{A_1(f)}{A_2(f)} + j \frac{\Phi_1(f) - \Phi_2(f)}{l_1 - l_2} \quad (1)$$

where $\mathbf{a}(f)$ and $\mathbf{b}(f)$ are the frequency-dependent attenuation coefficient and phase constant, respectively, $A_i(f)$ and $F_i(f)$ ($i = 1, 2$) are the amplitude and phase of the transforms corresponding to line lengths l_1 and l_2 , respectively, with $l_1 > l_2$. No de-embedding or calibration is required since the effect of interface discontinuities simply cancel out. The characteristic impedance can be obtained from:

$$Z_o(f) = \sqrt{\frac{R + j\omega L}{G + j\omega C}} = \frac{\Gamma(f)}{G + j\omega C} = \frac{\mathbf{a}(f) + j\mathbf{b}(f)}{j\omega C(1 - j \tan \mathbf{d})} \quad (2)$$

and also $R(f)$ and $L(f)$:

$$R(f) = \text{Re}\{\Gamma Z_o\} \text{ and } L(f) = \frac{1}{\omega} \text{Im}\{\Gamma Z_o\} \quad (3)$$

For most of the insulators used in these cables, $G \ll \omega C$, which is in fact a requirement for high-speed signal transmission, and so (2) reduces to:

$$Z_o(f) \cong \frac{\mathbf{b}(f)}{\omega C} - j \frac{\mathbf{a}(f)}{\omega C} \quad (4)$$

If we further assume that C is frequency-independent and accurately measure the line capacitance at 1 MHz, the complex impedance can be extracted with great accuracy. Because of the low-frequency C measurement, any errors caused by parasitics of leads, probes, and pads are greatly reduced and the results have an accuracy of $\pm 1\%$. The corresponding accuracy of the impedance measurements is $\pm 2\%$ for the real part and $\pm 3.8\%$ for the imaginary part. The magnitude of the impedance will be primarily determined by the real part. Figs. 8a and 8b show the measured and calculated attenuation for the cables of Figs. 1 and 3, Fig. 9 shows the complex impedance for the cable of Fig. 1 and Fig.10 compares the odd-mode and even-mode attenuations for the AWG26 and AWG24 cables of Figs. 1 and 2. Table I lists the measured attenuations for the three cables for the odd-mode case. Even though the AWG24 cables have 23.8% larger signal diameter than the AWG26, the stranded construction results in attenuation differences that are larger at lower frequencies, but then decrease at higher frequencies. The AWG24 cables show much less even-mode attenuation due to the heavier braided ground shield compared to the use of only a smaller diameter wire for the AWG26 ones. Finally, the RG400 cables, show the smallest losses.

Due to the extremely high loss found for the even-mode of excitation when the return is through the resistive drain wire and foil for the AWG26 cables, the short-pulse measurement was performed with 12.7-cm- and 38-cm-long lines. All the odd-mode measurements for all the cables were performed with 1-m- and 3-m-long cables. The odd-mode attenuation was calculated in all cases and iterated until agreement with measurement was obtained by varying the assumed \mathbf{tand} . For the AWG26 cables of Fig. 1, $\mathbf{tand} = 0.00075$ gave the best fit. The manufacturer specified a lower value of $\mathbf{tand} = 0.00045$. The RG400 cables were found to have $\mathbf{tand} = 0.00016$ up to 2 GHz and an equivalent $\mathbf{tand} = 0.0006$ up to 31 GHz. The attenuation obtained for the AWG24 cables was found to be extremely similar to the data supplied by the vendor. The vendor data was obtained using network-analyzer-based frequency-domain measurements [13].

III. Cable Modeling

The cross sectioning of the cables that are shown in Figs. 1-3 provided the correct dimensions. The conductor resistivity was obtained by using the dimensions and the four-point resistance measurements. The capacitance was calculated using a modified version of the numerical technique described in [14] that can handle multi-faceted polygon cross sections. The circular conductors were approximated by 64-sided polygons. By assuming a uniform dielectric, the high-frequency inductance, L_∞ , was also obtained from the inverse of the capacitance matrix since the propagation delay per unit length for a uniform dielectric and homogenous, lossless case is $\mathbf{t} = \sqrt{LC} = \sqrt{\mathbf{em}}$, where \mathbf{e} and \mathbf{m} are the dielectric constant and permeability of the medium, respectively. The differential cables were treated as two, symmetric, coupled lines, and thus 2×2 , capacitance, C , and inductance, L , matrices were

obtained. For the odd-mode excitation, $C_{odd} = C_{11} + C_{12}$, where $C_{11} = C_{22}$, and $L_{odd} = L_{11} - L_{12}$, where $L_{11} = L_{22}$. $R_{odd} = R_{11} - R_{12} = R_{10}$, or the resistance without the return since ideally there is no current return through the braid conductor. In the case of the even-mode excitation, the current will return through the shield, so $R_{even} = R_{10} + 2R_{12}$ and will increase significantly. R_{12} in all cases is the effective drop of the return path. $C_{even} = C_{11} - C_{12}$ and $L_{even} = L_{11} + L_{12}$. Since

$$Z_{odd} = \sqrt{\frac{L_{11} - L_{12}}{C_{11} + C_{12}}} \text{ and } Z_{even} = \sqrt{\frac{L_{11} + L_{12}}{C_{11} - C_{12}}} \quad (5)$$

the Z_{even} impedance is much higher than Z_{odd} as the measurements show in Fig. 6.

For $f = 16.4$ mils and $r = 1.837$ $mWcm$, skin-effect onset (where $d \leq 0.3f$) will occur for frequencies as low as 0.3 MHz. This implies that we can assume skin-effect to be present throughout the entire frequency range of interest. Wheeler's incremental inductance rule [11, 15] can then be used to calculate $R(f)$ and $L(f)$ matrices. Due to skin-effect, current crowding on the surface of the conductor increases its effective resistance. This surface resistance R_s is equal to the change in inductive reactance caused by the penetration of magnetic flux into the conductor when $d \ll f$, an approximation valid in all our cases. So $R_s \cong X = wL_{int}$ where L_{int} is the internal inductance. So:

$$R(f) = R_s(f) = w \frac{d}{2} \frac{\partial L}{\partial n} \quad (6)$$

and

$$L(f) = L_{ext} + L_{int}(f) = L_{ext} + \frac{d}{2} \frac{\partial L}{\partial n} \quad (7)$$

where n is the direction normal to the surface and L_{ext} is the external inductance. The change in inductance $\frac{\partial L}{\partial n}$ when penetration occurs at $d/2$ from the surface can be obtained from two capacitance calculations, one at the surface and one assuming that all the surfaces recede by $d/2$. The rate of change $\frac{\partial L}{\partial n}$ can thus be derived. A three-point fit was actually used for AWG26 cables, with the inductance calculated at the surface, 0.1-mils, and 0.2-mils from the surface. In this case, since the signal conductors were made of copper and the shield of aluminum, skin-depth was scaled by the ratio of resistivities, namely 2.64/1.837, since the penetration is stronger into the shield. Thus all the $R(f)$ and $L(f)$ matrix terms are computed analytically using (6) and (7) and the numerical technique of [14] that yields $L_{\infty} \cdot L_{ext}$ is obtained from the relation $LC = \epsilon m$ calculated in free space.

Since the low-frequency range is limited in the short-pulse-technique to about 0.3 GHz, additional low-frequency data points were obtained by using 10-cm cables and measuring R and L down to 10 MHz. Both the HP4275A Multi-Frequency LCR meter and the HP4194A Impedance/Gain Phase Analyzer were used in a four-point impedance measurement arrangement. The 10-cm-long cables were wired to mimic either the odd-mode or even-mode excitations. For the odd-mode, the output signal cable ends were shorted together and the + and - signals were driven through the two signal input ends. For the even-mode, both ends of both signal lines were driven in parallel. The output end was then connected to the output end of the ground line and the input end of the ground line was the other signal connection to the meter. These points were added to the ones obtained from the short-pulse measurement. For the odd-mode attenuation, a circuit was synthesized to fit this entire extended frequency range and then extract $R(f)$ and $L(f)$. The results shown in Fig. 8a indicate that although $tand = 0.00075$ is quite small, the dielectric losses could become significant contributors to overall loss above 1 GHz.

The model used for simulations was derived by using a decoupled-mode transformation. Two symmetric coupled-lines can be reduced to two uncoupled single lines using linear voltage-dependent current sources [16]. Each line represents either the odd mode or the even mode of propagation. The final model has two such models that are very different because of the lossy return. For the even-mode model, the synthesized circuit was fit only up to 1 GHz due to the very large losses measured and shown in Fig. 10. Extending the fit above 1 GHz was

generating numerical convergence problems in the simulation. This frequency restriction was not used for the odd-mode model, since for + - excitation very fast signals can be propagated on these cables.

In the case of the RG400 cables, R and C were measured and the attenuation was extracted up to 10 GHz. Based on the cross sectional dimensions shown in Fig. 3, the obtained attenuation, and the dielectric loss specified by the vendor, the calculated attenuation was fit to measurements up to 2 GHz. The calculation was based on analytical formulas for circular coaxial cables [17]. Above 2 GHz, the fit could not be obtained unless additional factors were included, such as the tinned copper metallization and stranded cross section. Gradually increasing terms were added to the calculated attenuation to allow for a 10% increase due to the irregularity of the braid that behaves similarly to a rough surface and could generate additional longitudinal modes of propagation. 20% increase was attributed to the stranded construction. Below 5 GHz, the losses were considered mostly resistive, while above, the $\tan\delta$ increase accounted for the other effects resulting in a maximum $\tan\delta = 0.0006$ at 31 GHz and the results are shown in Fig. 8b. TDT measurements resulted in propagation delay of 47.3 ps/cm on short cables that translates into a dielectric constant of $\epsilon_r = 2.0$. This was similar to the vendor specifications for these cables.

IV. Card Wiring Analysis

Card wiring contributes significant loss and distortion to overall signal paths and therefore needs to be carefully designed and analyzed. Single and coupled line test structures were analyzed on test cards built with Getek [18] material. This material has gained popularity recently due to its low dielectric loss and mechanical properties. Fig. 11 shows the layout for some of the card wiring sites. Various line lengths were included, with and without vias along the length, and parallel plate capacitors for extracting the dielectric constant of the insulator.

The characterization followed the same procedure used for the unassembled cables. Cross sectioning sites shown in Fig. 11d were used to determine the actual card dimensions that are shown in Figs. 12 and 13. The copper resistivity was extracted to be $r = 2.09 \text{ m}\Omega/\text{cm}$. The dielectric constant was extracted from measurement of capacitance at 1 MHz of the 2.54-cm-diameter plate (shown in Fig. 10c) placed on the signal layer between the two ground planes of the strip-line card structure. It was found to be $\epsilon_r = 4.272$.

Single and coupled line capacitance measurements resulted in very good correlation with calculation as listed in Table II. The lines that were surrounded by vias had two configurations, namely GS and SSG. The GS vias had 43-mil capture pads on the signal layer and were placed on 2-mm-pitch along the length. The SSG vias had capture pads only every third position, on 6-mm pitch. All vias were 27-mil in diameter and were 5.37-mil away from the edge of the lines. The effect of the vias was modeled with a three-dimensional (3D) electromagnetic field solver [19] and it was found to be very small. Vias increased the self capacitance by +1.98% and +0.36% for GS and SSG cases, respectively, and decreased the mutual capacitance by 0.6% and 0.12%, respectively. Fig. 14 shows the 3D model used with the top ground plane removed for the GS case. The effect of vias is of concern because there are many instances where signal lines have to escape from underneath chip-carrier I/O areas or multi-row pinned connectors and the characteristics of the transmission lines could be altered compared to the open area where there are no vias. The mismatch in impedance values in such cases could generate additional reflections [12]. This was not found to be the case for the design that was used in Fig. 11 because of the large via-to-line separations.

Table III summarizes the characteristic impedance measurements and calculations. Calculations were performed with either 2D [14] or 3D [19] numerical technique. The measurement was performed with both the short-pulse technique and TDR using the 20-GHz sampling oscilloscope with $t_r = 30$ ps risetime, and for both odd-mode and even-mode excitations. The largest discrepancies in Table III are attributed to cross sectional non-uniformity that are evident in TDR traces. The implicit assumption in the short-pulse measurement technique is the uniform transmission line characteristic. The cross section assumed in the calculation was obtained from a limited sample sectioning. The average cross section assumed, based on sectioning, for example, was 8.5% narrower than the nominal design specification of 7.5-mil. The 45.7-cm-long lines had 10-cm-long sections with vias at both ends and no vias in the center 25.7-cm-long section. Fig. 15 shows the TDR traces for the 45.7-cm-long lines in both odd-mode and even-mode excitation. Once again, the effect of the adjacent vias is found to be minimal.

The short-pulse propagation technique was used with 4.9-cm- and 8.2-cm-long single lines to extract the attenuation, phase constant, complex impedance, $R(f)$, and $L(f)$. The best fit to the measured attenuation was obtained for $\tan\delta = 0.0075$ up to 2 GHz and $\tan\delta = 0.012$ above this frequency. Note that the attenuation in Table I at 3.162 GHz for the card wiring is 0.1226 dB/cm, while for the AWG26 cables is 0.0167 dB/cm, for the AWG24 cables is 0.0137 dB/cm, and for the RG400 cables is the lowest, namely 0.0080 dB/cm. This is why cable length are more than an order of magnitude longer than card wiring traces in actual use. Fig. 16 shows the measured and calculated card wiring attenuations. Notice the large contributions dielectric losses have to the total loss over our frequency range of interest.

V. Performance Analysis

a. Unassembled Data Cables

Signal propagation with either step or pulse sources was performed for all the cables and card lines and compared to simulations. This provided verification of the developed models. Fig. 17 shows such correlation for the AWG26 cables with 3-m- and 10-m-lengths driven by a 500-ps-wide pulse in odd-mode excitation, meaning one positive going pulse and one negative pulse. Only the positive going propagated pulse is shown. This corresponds to 2 Gb/s application. It should be noted that at 10-m-length, the signal risetime for a step excitation deteriorates to 1.2 ns due to both skin-effect and dielectric losses. It is recommended in [12] for the signal risetime t_r to be kept less than one third of the pulse width p_w for adequate signal integrity and for the total attenuation on the signal path to be less than 3-5 dB at the upper-3-dB frequency, f_c , where f_c and the propagated risetime are related as follows:

$$f_c = 0.35 / t_r \tag{8}$$

$$t_r \leq p_w / 3 \tag{9}$$

$$a_{TOT} \leq 3 - 5dB \tag{10}$$

For the step excitation and propagated $t_r = 1.2$ ns, $f_c = 0.29$ GHz. At 0.316 GHz, the total attenuation, a_{TOT} , in Table I for the AWG26 cable for $l = 10$ m is 5.4 dB. This is why the amplitude of the 500-ps-wide pulse degrades by 50% in Fig. 17. For 500-ps-width data pulses, the propagated step response risetime should not degrade to more than $t_r = 167$ ps. To overcome such restrictions, such cables are then generally used with pre-emphasis that is built into the driver circuit, passive equalization included in the connector or in the cable [13], or adaptive receiver equalization. The circuit approach will add more power dissipation, delay, and complexity in order to increase the driving signal amplitude and is optimized for the maximum cable length. The passive equalization requires a more complicated cable build and thus increases the cable cost and increases loss. In both cases, the high-frequency attenuation is the same but the bandwidth is increased due to increase in either the low frequency attenuation (for equalization) or increase in high-frequency spectrum (for-pre-emphasis). This operation is equivalent to superimposing a high-pass filter on the driving signal. The attenuation will increase more gradually at the high-frequency limit than the \sqrt{f} dependence. Because of the higher loss at low frequencies, long strings of 0s in the data are not favored and encoded data (most popular being the 8/10 bit version) is generally used and thus not affected as much. The 8/10B encoding also reduces the sensitivity of the signal integrity to the random data-pattern effect or the inter-symbol-interference (ISI) because it ensures that there are never more than five consecutive 1s or 0s. Both pre-emphasis and encoding help increase the "eye-opening" or the valid data window by enlarging the amplitude and width of the "eye" [20, 21].

Fig. 18 shows the results for even-mode excitation for much shorter lengths of 12.7 cm and 1 m. The difference is quite dramatic and is caused by the excessive even-mode losses shown in Fig. 10. The even-mode losses affect the signal characteristics when there are differences between the two paths, the + or the - of the differential pair. This can be due to unevenness in connectors, driver circuit skews, and chip-carrier leads and wiring. The fact that the attenuation is so high for the AWG26 cables in even-mode can actually be beneficial in reducing timing skew.

Timing skews will generate some partial current return through the resistive ground and thus slow down the signal transition and reduce signal amplitude. Timing skews could be generated by circuit, cable, or connector differences. These skews will be damped by the even-mode attenuation.

Figs. 19 and 20 show signal propagation results with the AWG26 cables with 3-m and 6-m lengths, for 1.19-ns-, 596-ps-, 334-ps-widths, and odd-mode pulse excitation. These correspond to 840 Mb/s, 1.68 Gb/s, and 2.99 Gb/s data rates. In all cases, the sources were two pulses of opposite polarity having 123-mV swing and 32-ps and 37-ps rise and fall times. Fig. 21 shows results for the AWG24 cables for 334-ps-width pulses. Skin-effect and dielectric losses affect the higher frequency components of the signal transitions the most [20] and give rise to the rounding of the upper part of the pulse transition. As the pulses become narrower, this rounding begins to reduce the steady-state level. The pulse width measured at the mid-swing level is affected much less by this dispersion. In the case of a random data pattern, the signal distortion is exacerbated. This is a result of each pulse having a variable starting level, depending on the number of consecutive low or high states (0s or 1s) preceeding it. This history effect is sometimes termed inter-symbol-interference or ISI. This is becoming increasingly significant for the high data rates encountered or planned. In a continuous string of data, the “eye-opening” will be reduced both in height and width. Generally, an “eye-mask” is defined (time and amplitude window during the cycle time when data can be reliably sampled). This eye-mask allows for a reasonable minimum signal at the receiver to overcome all the noise sources present in the system, such as crosstalk, simultaneously-switching-noise, or common-mode noise. The width will effect the sampling time range inside the eye-mask and will be affected by circuit and power supply tolerances, temperature variation, receiver threshold variations, path skew caused on chip or on the package and overall jitter. The various noise sources have to be contained within the receiver circuit noise margin in order to avoid logic failures.

Table IV defines a methodology for comparing the performance of various cables. Pulse propagation measurements were made with 334-ps-, 596-ps-, and 1.19-ns-wide pulses, in an odd-mode excitation, + -. The peak-to-peak amplitude of the input and propagated pulses are compared and listed in percentage compared to the source that has 100% amplitude. In the case of the eye-opening determination, this would give an indication of the height of the eye. The pulse widths are similarly compared with the starting source value. The width is measured at the 50% level since this is generally the switching threshold level for the receiver circuit. This will affect the horizontal width of the eye-opening. Finally, the risetime is reported around the switching level, $\pm 10\%$ around the middle of the signal. This is reported in actual value. Such a parameter is useful to give an indication of the expected jitter that would be of concern for clock paths. The slower the transition through this switching band, the higher the timing uncertainty. The $\pm 10\%$ band is probably pessimistic since the receiver threshold variation is closer to only $\pm 3\%$. The additional band could, however, be caused by other system tolerances. The sources for the three cases covered in Table IV had rise and fall times of 32 ps and 37 ps, and swing of 119 mV for the 334-ps case and 123 mV for the 596-ps and 1.193 ps cases.

Several factors can be noted from the results of Table IV. There is very little difference in propagated pulses for the AWG26 and AWG24 cables for lengths of 1 – 6 m even though the AWG24 cables have larger conductors. This lack of improvement is due to the use of the stranded construction. The very small decrease in attenuation seen in Table I is not significant and results into similar signal propagation characteristics. There is 12% longer delay with AWG26 cables because of the higher dielectric constant material used, namely 1.65 vs. 1.3. The difference is proportional to the ratio $\sqrt{\epsilon_{r1} / \epsilon_{r2}}$ and it is generally not of concern in typical applications where many cycles are transmitted on the cables. It is the signal integrity that affects the system performance and not the latency on the path. From the waveforms shown in Figs. 19, 20, 21, and Table IV, it seems that for 2.99 Gb/s data-rates (334-ps data pulses), cable lengths cannot exceed 2.7 m without the use of pre-emphasis or equalization. For 1.68 Gb/s, lengths can only go up to about 3.5 m, while for 840 Mb/s, lengths of 5.2 m can be used. Fig. 22 summarizes the above prediction. Fig. 21 shows the waveforms for 2.99 Gb/s for $l = 1, 3,$ and 6 m that were measured. From the relations given by (8) and (9), for 334-ps, 596-ps, and 1.19-ns wide pulses, the needed risetimes are 111 ps, 199 ps, and 396 ps, respectively and $f_c = 3.2$ GHz, 1.76 GHz, and 0.88 GHz. The maximum path attenuation recommended by (10) is 3-5 dB. For $a_{TOT} = 4.5$ dB, the maximum useable lengths at 3.2, 1.76, and 0.88 GHz are 2.65 m, 3.5 m, and 5.2 m for the AWG26 cables. From Table IV this corresponds to a swing of

85%, or $\pm 7.5\%$ loss of steady-state level. This is generally considered acceptable since most receiver circuits have a noise margin of $\pm 40\%$. The RG400 cable prediction shown in Fig. 22 will be explained later.

The data rate, DR, deteriorates somewhat faster than the relation $DR \propto \frac{f^2}{J^2}$ [22] in Fig. 22 that is predicted for skin-effect induced resistive losses. This increase is attributed to the additional increase in attenuation due to dielectric loss and the non-ideal transmission-line constructions used in Figs. 1-3. In actual use, for typical applications, such as the Infiniband case, the cable would contain equalization circuitry to compensate for 6-10 dB of loss at 2.5 Gb/s to result in a jitter J caused by ISI to be one quarter of the bit time, BT, or 100 ps ($J = 0.25 BT$). The actual path will have additional losses from the card wiring and the other connectors and chip carrier traces and connections. The signal shown in Fig. 17 sees only the effect of the unassembled cable and has no pre-emphasis or equalization to improve the shape. It should also be noted that the height and width of the data window is very much system design dependent. It is influenced by the design, timing, and routing of all the components in the signal path. The size of the window will be affected by these effects and further restrict the lengths predicted in Fig. 22. Distortions caused by reflections from connectors and other discontinuities in the path will also reduce the width. The lengths and data-rates shown in Fig. 22 are considered extremely restrictive for typical applications. Compensation is routinely used for data cables. These measurements of the uncompensated cables, however, evaluate the various cable technologies and thus guide the system designer in the required compensation.

b. Unassembled Clock Cables

In the case of clock paths, where the clock signal needs to be distributed to all the critical nodes with zero skew and minimal jitter, the signal requirements are even more stringent than for data paths. The actual latency is not critical as long as it is equal for all the branches. Since clock paths are routed in special, custom channels, the likelihood of noise-induced distortions is less. Oftentimes, such clock signals are driven by bipolar drivers that are much more insensitive to power supply fluctuations. In such cases, there is no random-data transmission, rather a continuous string of pulses is used that should maintain symmetry of switching, or 50% duty cycle, since switching could occur on both edges of the clock signal. The most important parameter to control is the edge-rate characteristic through the switching threshold that could be $\pm 3-10\%$ around this level. This is the value that was listed in Table IV, as risetime in the 40-60% band. Fig. 3 shows possible cables that could be used for clock applications. In this case, single RG400 cables are used in delay-matched differential pairs. Due to the larger diameter construction, the attenuation that was measured was much less than for the other cables in Figs. 1-2 as it is shown in Table I. Actual testing of pairs of cables revealed that delay through pairs could be matched within 5 ps. Measurement uncertainty is considered to be ± 1 ps. Ten differential pairs were measured to have a skew of ± 2 ps. The vendor specification was ± 5 ps. The measurement was performed with the 20-GHz HP 54120 sampling oscilloscope and connectorized cables. The oscilloscope has a 50 GHz bandwidth detector and the cables use SMA connectors. Measurements were repeated three times to ascertain the uncertainty.

The cable models that were obtained from the short-pulse measurements described earlier were used in signal simulation. Step-source and pulse-source measurement and simulation results show excellent agreement in Figs. 23 and 24. Results are shown for 3-m and 4.5-m long cables. In the case of the 500-ps-wide pulse, the signal transition used was 107 ps in order to more closely resemble the actual driver circuit output. The measurements in Figs. 23 and 24 were made with cables without the end SMA connectors. Due to the 107-ps source risetime, there is a 22.4 ps initial jitter supplied around the 40-60% band. In this case, the band is 19.4 mV and the total amplitude is 97 mV. The 3-m and 4.5-m cables exhibit 30-ps and 36-ps jitter in the same band or 2.9 V/ns. This then represents an increase of 13.6 ps in jitter over the source for the 4.5-m cable that is considered extremely good.

For the step source, the 10-90% propagated risetimes are 97-ps and 135-ps for the 3-m and 4.5-m cables. These risetimes are much improved over values obtained with the AWG26 and AWG24 cables. The 97-ps and 135-ps transitions correspond to a data rate of 3.4 Gb/s and 2.4 Gb/s, respectively. In this case, the total attenuation is 2.8 dB and 3.6 dB, respectively, because the desired edge rate was faster. The 40-60% band is especially important for the clock path usage. The voltage swing is also better in this case but it is not the main consideration for cable selection. The penalty for such cables is the increased cost in building phase-matched (delay-matched) individual

cables and the bulky mass of the larger diameters. Clock cables, however, tend to represent a small percentage of the total cables in typical parallel system environments. Large-gage differential cables can be built but their construction is also much more difficult. Because there are only a few clock cables in the system, the connector pin density is not of concern as it is in the case of the large bundles of data cables. It should also be noted that the RG400 cables shown in Fig. 3 are about the largest size that would be practically considered for high speed signal transmission. While $Z_0 = 50 \Omega$ design could be obtained with larger diameters, the overall cross sectional dimensions will tend to approach the signal wavelength for fast transitions and non-TEM modes of propagation, such as circular waves, could develop and distort the signals [23].

c. Card Wiring

The card wiring dimensions and lengths are carefully designed to introduce minimal additional distortions. Nevertheless, physical constraints imposed by connectors, chip carriers, decoupling capacitors, heat sinks, shields for EMI, card-to-card distance in a rack, and cooling requirements restrict the flexibility of the design. The cross sections that were analyzed in Figs. 12 and 13 are more typical for paths that have long cables. Typical card wiring dimensions for intra-system communication use 3-4-mil line widths. As the data rates are pushed to higher speeds, the card line dimensions are increasing in order to reduce resistive losses. New materials, with lower dielectric loss, are adopted, and technologies that allow for smaller, not drilled vias, need to be used because thick cards, with long, and wide vias generate very large discontinuities along the path and thus distort the propagated risetimes. This is why new manufacturing techniques are being introduced.

Fig. 25 shows the good correlation obtained between measured and simulated waveforms for the coupled-line card wiring of Fig. 11. Measurements were made with odd-mode excitation and 52-ps-risetime step source. The line resistance is $R = 0.038 \Omega/\text{cm}$ while for the RG400 cables we measured $R = 0.00029 \Omega/\text{cm}$.

VI. Full-Path Analysis

The full-path from the driver to the receiver circuit will traverse some on-chip wiring, solder-ball or wire-bond connection to a chip carrier, carrier wiring that can be ceramic- or polymer-based, pins or solder-balls for connection to the card wiring, considerable card length, card-to-board connector, and chip carrier for the receiver circuit. Other configurations, with more card-to-board transitions or having the cable driver and receiver carrier on the same card are sometimes used. The impedance mismatch between the cable and card wiring and these discontinuities cause reflections that will further distort the signal transitions beyond just the resistive and dielectric losses. The differential signaling helps reduce the effect of these reflections on the differential signals at the receiver but it does not eliminate them. These interfaces, in fact, are the ones that contribute to the most imbalance between the + and - going signals and thus some residual ++ or even-mode transmission occurs. This is why it is important to analyze representative portions of a full-path.

The AWG24 cables were tested in a path where the connectors were attached and a short length of 1.72-cm length of card wiring was also included at both ends. The coaxial probes attached to probe pads that had vias connecting to the card wiring in a strip-line configuration. Vias also connected the card wiring to the cable connectors. The Quietzone connector [7] on 0.1-inch pitch was used as shown in Fig. 26. The connector carries the shielding of the two signal lines all around the connector contacts, however, the ground connection to the card is through only one additional ground pin on one side as also seen in the top view layout of Fig. 11f. This then creates an imbalance in the cable-to-card transition between the + and - paths if there are any ++ components present due to driver signal skew. Figs. 27, 28, and 29 show the propagated waveforms for 334-ps-wide pulse in odd-mode excitation, with and without connectors. The largest distortion is introduced for the shortest, 1-m-long, cables that propagate the fastest signal transitions, while the 6-m response is quite similar with or without connector. For the 1-m-long cables, the risetime increases from 69 ps to 114 ps, for the 3-m-long cable it goes from 142 ps to 159 ps, and for the 6-m-long cable the transitions are 195 ps and 198 ps. It is concluded then, that in the case of very long paths, the cable and card wiring will contribute the most to risetime distortion. As the data rates are increased and shorter lengths are needed and accommodated by higher package integration or use of re-buffering, the faster

transitions will be affected more by these other discontinuities. That is when the cable discontinuities will become important. The 69-ps and 114-ps transitions for $l = 1\text{m}$ correspond to 2.9 and 4.8 Gb/s data-rates.

Measurements were also made with the RG400 cables in a full-path configuration as shown in Fig. 30. In this case, two sections of 5-cm-long card wiring of the type shown in Fig 11 were included at each end of the cables. Fig. 11g shows a top view of the layout for this test site. The SMA connectors that were attached to the card had a 90° bend and a bulk-head adapter that is also often used for connecting to a shielding enclosure. Fig. 31 compares the measured and simulated waveforms based on the card and cable models that were discussed earlier. The cable connector discontinuities are introduced in the simulations as well. These additional inductance L and capacitance C values were obtained from best fitting to TDR waveforms. The step source transition had $t_r = 52\text{ ps}$. The measured delay, risetime, and swing for 4.5-m-long cables in odd-mode excitation were 22.31 ns, 300 ps, and 245.7 mV. The respective simulated values were 22.1 ns, 290 ps, and 248.2 mV, so the agreement is considered quite good. Pulse measurements were also performed with 749-ps-width, in odd-mode excitation. This is representative of 1.34 Gb/s data rate. The results were also compared to the case where the AWG24 cables were used instead.

Since the RG400 cables were mostly considered for clock distribution, the transition Dt through the $\pm 10\%$ band around the mid-signal level was considered most significant. The + and - waveforms are shown for one single pulse. In actual clock signaling, a train of pulses would be used. The source transitions in this case were 36-ps (between 10-90% levels), while the actual driver circuit could generate 100-150-ps transitions. The Dt parameter, nevertheless, gives a good indication of the relative performance of the different technologies being evaluated.

Fig. 32 compares the propagated pulses for 5-cm and 45.7-cm card wiring. The source has $Dt = 9\text{ ps}$ for $t_r = 36\text{ ps}$. The 5-cm wiring increases Dt to 14.4 ps and the 45.7-cm-long wiring increases this parameter to 37.4 ps. The signal transitions were $t_r = 122\text{ ps}$ and 262 ps that is quite substantial degradation for the 45.7-cm card wiring. The presence of the vias along the card wiring has very minimal effect as shown in Table V. The 4.5-m-long RG400 cables were also connected directly to the oscilloscope inputs and outputs. The bulk-head adapters were included. In this case, $Dt = 19.2\text{ ps}$ and $t_r = 206\text{ ps}$. For the 3-m-long RG400 cables, $Dt = 11.6\text{ ps}$ and $t_r = 128\text{ ps}$. The transitions measured without any connectors were $t_r = 97$ and 135 ps for 3-m- and 4.5-m-long cables, respectively, and so the SMA and bulkhead connectors increase the risetime by 31-71 ps. Fig. 33 compares the results for the 5-cm wiring and the full-path with 10-cm wiring and 4.5-m RG400 cables. This full-path has $Dt = 49.2\text{ ps}$ and $t_r = 254\text{ ps}$ that is fairly close to the summation of the 10-cm-card and cable-only degradation. Removing the bulk-head adapters decreases Dt to 45.6 ps as seen in Table V. It was also found that a AWG18 differential cable, that was not shown here, exhibited $Dt = 48.5\text{ ps}$. In this case the signal cables had a diameter of 48 mil or 1.5 times larger area than the RG400 cables. The resistance was also 1.5 times lower than for the RG400 cables. The performance, however, was very similar, mostly due to the high dielectric loss of the polyethylene insulator used. Fig. 34 compares measured and simulated waveforms for the full-path and shows good agreement thus validating all our modeling. Finally, Fig. 35 shows the response for the same full-path and 4.5-m long cables, for RG400 and AWG24 cables. As can be seen in Table V, there is a 15.5% lower swing for the AWG24 cables that have $R = 0.001244\ \Omega/\text{cm}$ compared to the RG400 with $R = 0.00029\ \Omega/\text{cm}$. The signal-transition difference is 27.5% due to the increased losses and $Dt = 55.2\text{ ps}$. This is 19.5% higher for the AWG24 cables compared to the RG400 ones. There was also a 100-mils mismatch in card wiring length due to routing constraints, combined with the single-sided ground pin in the Quietzone connector that resulted in the 29-ps skew seen in Fig. 35 between the + and - signals arriving at the receiver. Fig. 11f shows a top view of the test site for this case. This is likely to introduce additional jitter even though the signal amplitude provides adequate data window.

The data-rates shown in Fig. 22 are for cables without connectors and are based on the condition given by (9) for the measured propagated risetimes. For the RG400 cables without connectors, $Dt = 9\text{ ps}$ and 12 ps for the two lengths shown and measured. This Dt values increase to 11.6 ps and 19.2 ps with connectors, and to 40.4 ps and 49.2 ps for the full-path with card wiring, connectors, vias, and cables. While the data-rates shown in Fig. 22 are 3.4 Gb/s and 2.47 Gb/s, for the full-path, the rates would be 2.6 Gb/s and 1.6 Gb/s if the propagated risetimes would be the limiting factor. As explained earlier, for clock cables, however, Dt is the most important parameter. The pulse amplitude and width are both much better than needed for a data-cable. The worst-case Dt exhibited by the longest cable anticipated in the system becomes the deciding factor. In this case, $Dt = 49.2\text{ ps}$ is the limiting performance parameter. The system designer needs to balance all the jitter contributions in the overall critical path

and define the needed jitter budget. Typically, such a budget could be 10-20% of the propagated risetime. So for 20% allocation, the jitter budget J for a target data-rate DR would be $J = 0.2 \times t_r = 1 / (15 DR) = 0.067 p_W = 0.067 \times BT$ based on (9). It should be noted that the jitter on the data-path cables could be much larger such as in the Infiniband specification of $0.25 \times BT$ or 100 ps for 2.5 Gb/s. For 1.4 Gb/s data-rate, the propagated risetime, based on (9), should be less than 238 ps, for example. Therefore the total Dt should be less than 48 ps. The RG400 cables that were analyzed here have a performance close to this target. This is then following the results of our recommendations. From (8) and Table I we have $f_c = 1.47$ GHz and $a_{1.47GHz} = 0.0055$ dB/cm for the cable and $a_{1.47GHz} = 0.048$ dB/cm for the card traces. The total path loss is then $a_{TOT} = 2.8$ dB for 4.5-m-long cable and 10-cm card wiring. This is then consistent with the measurements of Table V and Fig. 22. In this path, the dominant loss is caused by the cable since the driver and receiver circuits are assumed to be placed very close to the cable connectors.

VII Conclusions

A representative set of differential and single-ended shielded coaxial cables were analyzed. The analysis included 1-10-m lengths of cables for data rates of 0.84 Gb/s up to 3 Gb/s. These configurations are representative for present-day and near-term intra-system communication needs. The performance limiting parameters that were highlighted gave indications of the problems that will be encountered as the data rates are pushed toward 10 Gb/s.

The study included very careful analysis of the unassembled cables, the card wiring, and the effect of connectors and vias. Specially designed experimental structures allowed the extraction of material characteristics such as metal resistivity, dielectric constant, and dielectric loss. TDR measurements highlighted the cross sectional non-uniformities encountered on such long cable spans. Based on these experimentally obtained parameters, models were developed for all the card and cable wiring. Good agreement between measured and simulated waveforms on representative paths that included card and cable wiring validated the developed models. The coupled-line models that were developed allowed accurate simulations for performance evaluations for both odd and even excitations. This is essential in highlighting the effect of path timing unevenness and reflections. Single line, equivalent odd-mode simulations based on models fitted to vendor odd-mode measurements that are generally used, ignore all these additional distortions. The predictions in such cases can have large errors. Time-domain measurements were performed throughout for evaluating the interconnection performance. This is considered relevant for the digital signals that are being transmitted in actual use. Such measurements gave direct indication of signal rise-time degradation, delay, pulse width and jitter. A simple, short-pulse-propagation technique, performed also in the time domain, was used to extract the frequency-dependent resistive and dielectric losses and they were also included in the model generation process.

These losses were shown to be significant in all cases. Skin-effect losses were shown to be significant over the entire frequency range of interest and dielectric losses added significant distortion to the fast transitions used for the higher data rates. Both the card and cables used had fairly low dielectric-loss insulators. At the same time, however, the conductor resistance was low and so the combination of long lengths and desire to transmit the fast signals, made the dielectric loss add significant distortion. Long card wiring can have similar loss to long cables. This is why card connections between driver circuits and cables are generally kept as short as possible. As the signal transitions that are needed become shorter, the deteriorating effect of connector discontinuities increases. For slower signals on long interconnections, connectors and other discontinuities affect the risetimes much less compared to resistive losses.

It is important, then to analyze representative full-paths that include all the critical elements and to excite the interconnections with representative signals. The study used differential signaling that is being extensively used in present and future applications. Even-mode signal excitations highlighted the significantly higher losses that would be present. This then gave further motivation to designers to go to great length in avoiding any imbalances in the characteristics of the $+$ - traces of a differential path in order to avoid even-mode components. The unevenness of components in a full-path, the many interface discontinuities and impedance mismatches along the chip-to-chip path, and the dielectric loss and non-uniform and stranded constructions of these interconnections result in signal

propagation with data-rates that decrease faster than the relationship $DR \propto \frac{f^2}{l^2}$ predicted by skin-effect losses alone as was seen in Fig. 22. Circuit and coding techniques are able to extend these data rates at the expense of signal to noise ratio or driver power and complexity. The limited data-rates and lengths shown in Fig. 22 highlight the need for these compensating techniques and show the magnitude required. This study focused on the performance of uncompensated cables and evaluated their relative performance capability.

A methodology of evaluating these cables was indicated by the examples shown in Table IV. In the case of data-paths, the data valid window size requires the monitoring of the amplitude and the pulse width change as a function of length and data rate for a random data pattern. In the case of clock-signal paths, the signal transition through the switching threshold for a continuous string of pulses at the middle of the signal swing will affect performance the most. In these cases, the clock jitter will be directly affected by the slew-rate through this band.

Performance predictions need to rely on accurate models of all the components in the paths. This study has shown techniques of developing such models and what the key performance limiting parameters are. The study also showed that even with the very low-resistance card wiring, short card connections, large cable sizes, and very low dielectric-loss insulators, data rates will be difficult to increase. Designers will be using wider data buses, bi-directional signaling, many re-buffering stages to improve throughput. Innovative driver and receiver circuit and encoding techniques can give some boost but eventually the switch to optical interconnections will be inevitable.

Acknowledgements

The authors would like to thank Kenneth Scea from IBM Poughkeepsie and Sean Souffie and James Broomall from W. L. Gore & Associates for supplying the many cable samples used in our measurements and their frequency-domain data for comparison.

References

- [1]. M. LaPedus, "3.5 GHz Pentium 4", Semiconductor Business News, Aug. 28, 2001.
- [2]. <http://www.rapidio.org/>
- [3]. <http://www.infinibandta.org/background.html/>
- [4]. R. P. Luijten, "Future Interconnect Requirements in High-Speed Switches for Internet Backbones", *Proc. IEEE 9th Topical Meeting on Electrical Performance of Electronic Packaging, EPEP'98*, Scottsdale, AZ, Oct. 23-25, 2000, pp. 7-8.
- [5]. M. L. Schmatz, "High-Speed and High-Density Chip-to-Chip Interconnections: Trends and Techniques", *Proc. IEEE 9th Topical Meeting on Electrical Performance of Electronic Packaging, EPEP'98*, Scottsdale, AZ, Oct. 23-25, 2000, pp. 23-24.
- [6]. Spectra-Strip is Trademark of Amphenol Interconnect Products Corp., 20 Valley Street, Endicott, NY 13760, (607) 754-4444
- [7]. AWG24 cables and Quietzone connectors made by W. L. Gore & Associates, Inc., P. O. Box 8038, Newark, DE 19714
- [8]. Picoprobe 40A-GS-150-LP made by GGB Industries, Inc., P. O. Box 10958, Naples, FL 34101, (841) 643-4400.
- [9]. E. R. Hanson, G. K. G. Hohenwarter, S. R. Whiteley, and S. M. Faris, "Ultra-wide bandwidth instrument product based on Josephson junctions", in *Proc. Int. Conf. Computer Design (ICCD'87)*, Rye Brook, NY, 1987, pp.472-485.
- [10]. A. Deutsch, G. Arjavalngam, G. V. Kopsay, "Characterization of Resistive Transmission Lines by Short-Pulse Propagation", *IEEE Microwave Guided Wave Lett.*, vol. 2, no. 1, (1992), pp. 25-27.
- [11]. A. Deutsch, et al., "High-speed signal propagation on lossy transmission lines", *IBM J. Res. Develop.*, vol. 34, (1990), pp. 601-615.

- [12]. A. Deutsch, G. V. Kopcsay, P. W. Coteus, C. W. Surovic, P. Dahlen, D. L. Heckman, D. W. Duan, "Frequency-Dependent Losses on High-Performance Interconnections", accepted for publication in *IEEE Trans. on EMC*, Oct. 2001.
- [13]. J. R. Broomall, H. Van Deusen, "Extending the Useful Range of Copper Interconnects for High Data Rate Signal Transmission", *Proceedings 47th Electronic Components and Technology Conference*, May 18-21, 1997, San Jose, CA, pp. 196-203.
- [14]. W. T. Weeks, "Calculation of Coefficients of Capacitance of Multiconductor Transmission Lines in the Presence of a Dielectric Interface", *IEEE Trans. on MTT*, vol. MTT-18, no. 1, Jan. 1970, pp.35-43.
- [15]. H. A. Wheeler, "Formulas for the Skin-Effect", *Proc. IRE*, pp.412-424, 1942.
- [16]. V. K. Tripathi and A. Hil, "Equivalent Circuit Modeling of Losses and Dispersion in Single and Coupled Lines for Microwave and Millimeter-Wave Integrated Circuits", *IEEE trans. Microwave Theory Tech.*, vol. MTT-36, 1988, pp.256-262.
- [17]. R. E. Collin, *Foundations for Microwave Engineering*, McGraw Hill, 1966, Sec 3.2, p 79-89 (and Table 3.1 on p 81).
- [18]. Getek is a trademark of General Electric Electromaterials, 1350 South Second Street, Coshocton, OH 43812, (740) 622-5310.
- [19]. J. Rubin and S. Daijavad, "Calculation of Multi-Port Parameters of Electronic Packages Using a General Purpose Electromagnetic Code", *Proc. IEEE 2nd Topical Meeting on Electrical performance of Electronic Packaging, EPEP'93*, Monterey, CA, Oct. 20-23, 1993, pp.37-39.
- [20]. A. Deutsch, "Electrical Characteristics of Interconnections for High-Performance Systems", *Proceedings of the IEEE*, vol. 86, no. 2, Feb. 1998, pp. 315-355.
- [21]. J. Dally, J. W. Poulton, *Digital Systems Engineering*, Cambridge Univ. Pres, 1998, Ch. 8.
- [22]. D. A. B. Miller, H. M. Ozaktas, "Limit to the Bit-Rate Capacity of Electrical Interconnects from the Aspect Ratio of the System Architecture", reprint of Ginzton Laboratory Reort #5458, Stanford University, October 1996 to be published in Special Issue on Parallel Computing with Optical Interconnects, *Journal of Parallel and Distributed Computing*, 2001.
- [23]. R. E. Collin, *Field Theory of Guided Waves*, McGraw-Hill Book Co., Inc., New York, 1960, pp.343-373.

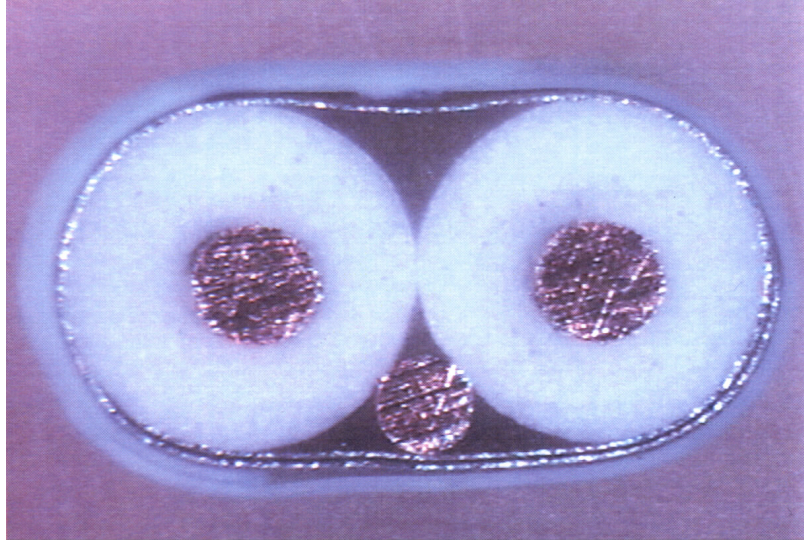


Fig. 1. Cross section of the AWG26 cables with two signal conductors, one drain wire, and a thin foil shield.

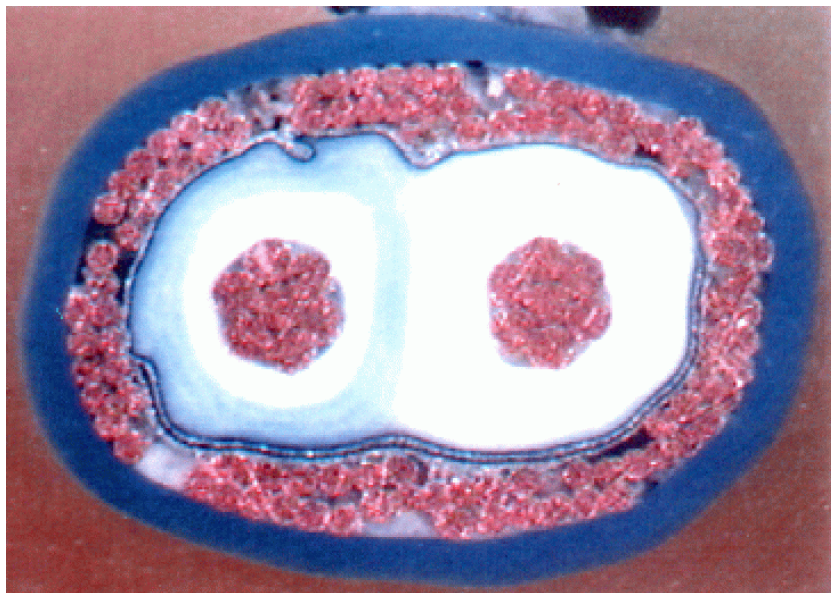


Fig. 2. Cross section of the AWG24 cables with two stranded signal conductors, a stranded external shield, and a thin foil underneath.

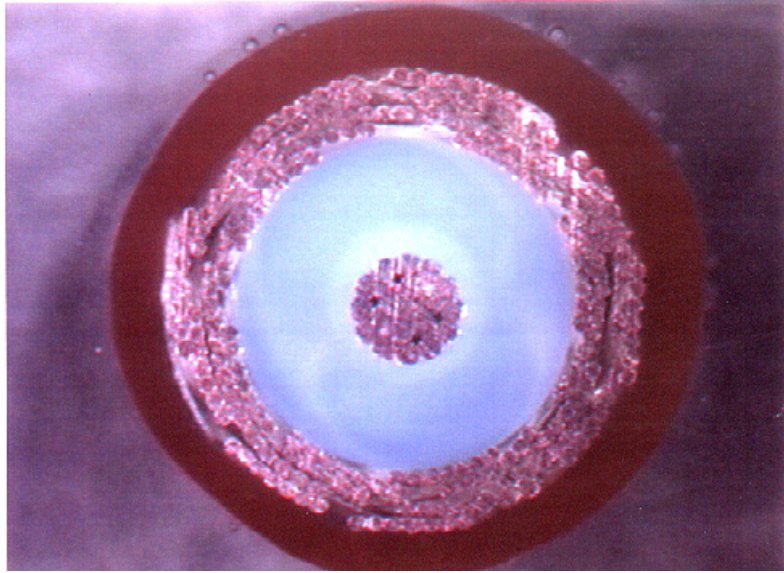


Fig. 3. Cross section of RG400 cables with stranded signal and outer shield.

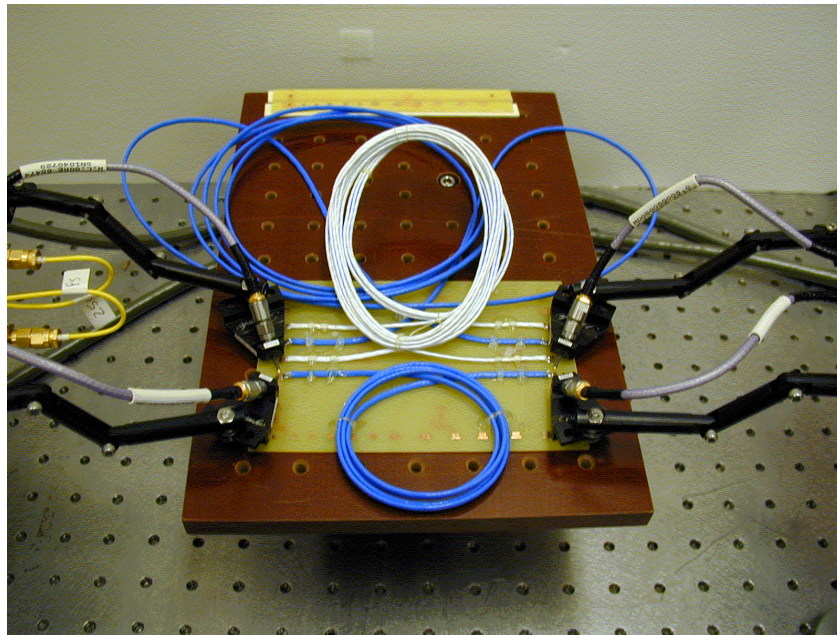


Fig. 4. Measurement set-up used for differential excitation and detection of either the AWG26 or AWG24 cables of Figs. 1 and 2 using a test card with the cables soldered to surface test pads.

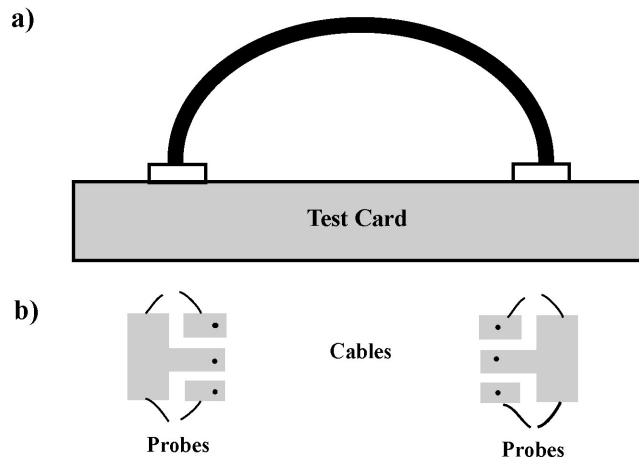


Fig. 5 Test card used for measuring unassembled cables. a) Cables are attached to top-surface test pads and b) a top view of the test pads shows the place where the coaxial probes are attached.

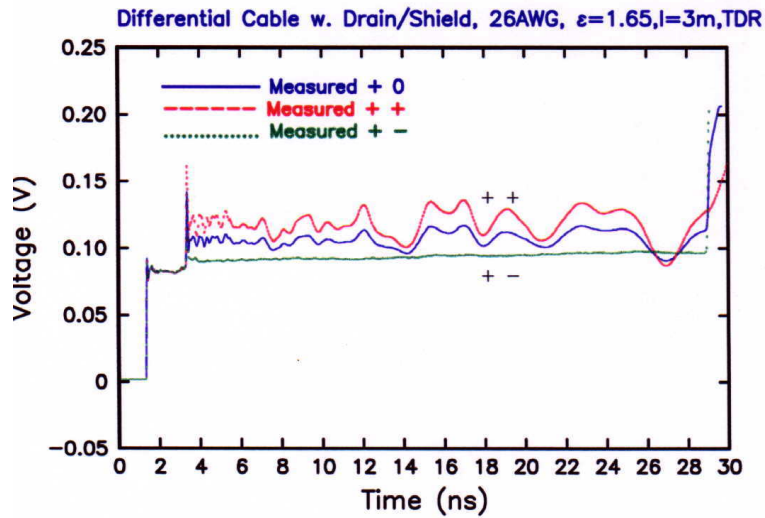


Fig. 6. TDR measurements of AWG26 differential cables with $l = 3\text{m}$, step source with 30-ps transition, and either $+ -$, $+ +$, or $+ 0$ excitation modes.

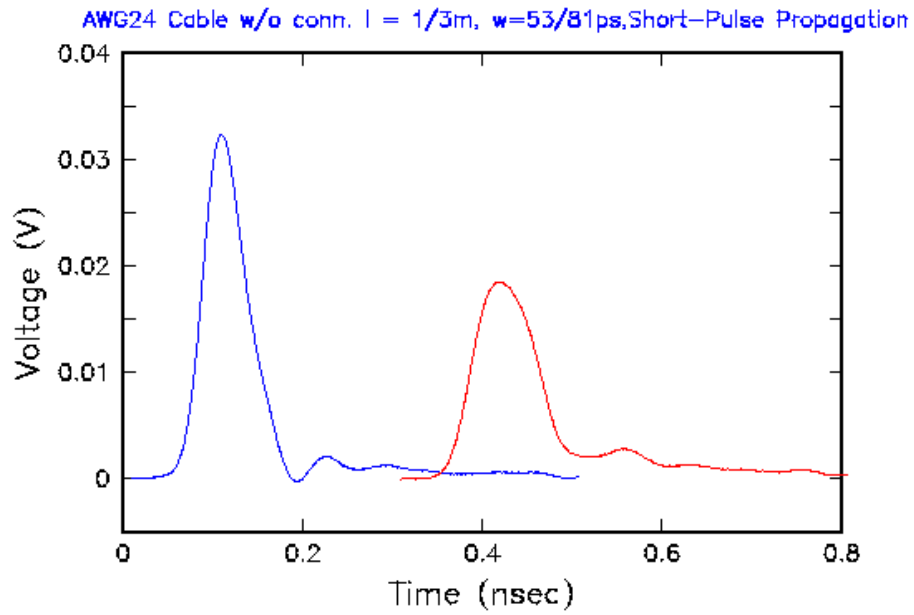
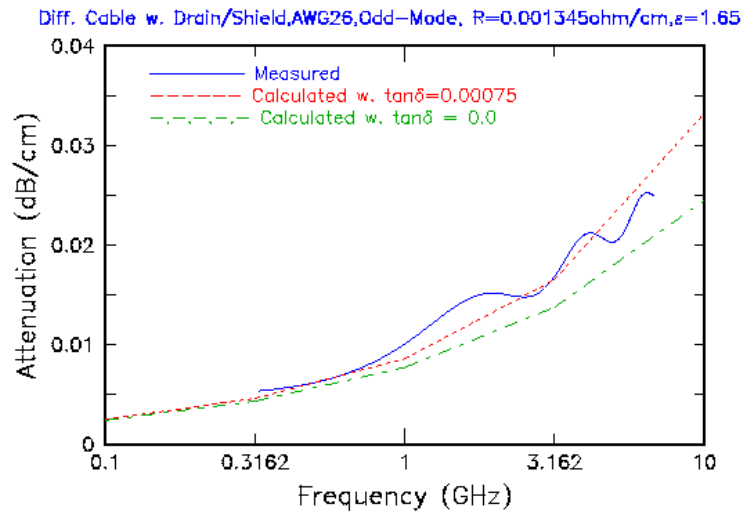


Fig. 7. Propagated pulses on the AWG24 cables of Fig. 2 for $l = 1$ m and 3 m that are used in the short-pulse-propagation measurement technique.



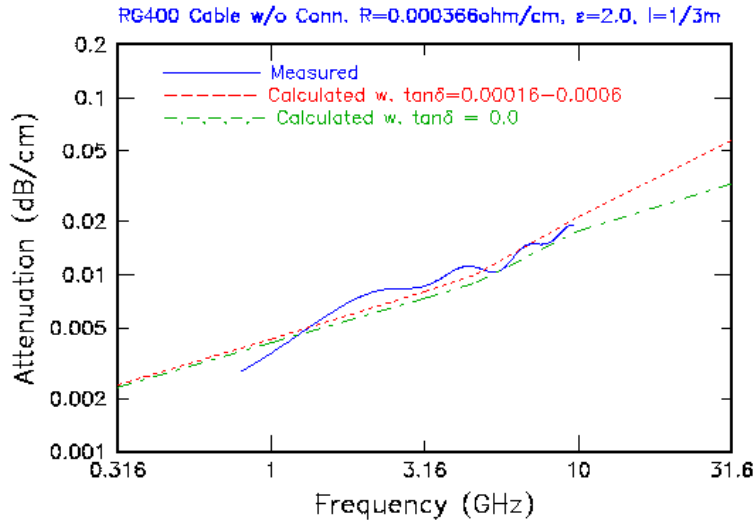


Fig. 8. a) Measured (solid) and calculated attenuation with $\tan\delta = 0.0$ (dot-dashed) and $\tan\delta = 0.00075$ (dashed) for the AWG26 cables of Fig. 1 and using the short-pulse-propagation technique with 1-m and 3-m long cables and odd-mode, + -, differential excitation, b) measured (solid) and calculated attenuation with $\tan\delta = 0.0$ (dot-dashed) and $\tan\delta = 0.00016 - 0.0006$ (dashed) for the RG400 cables of Fig. 3.

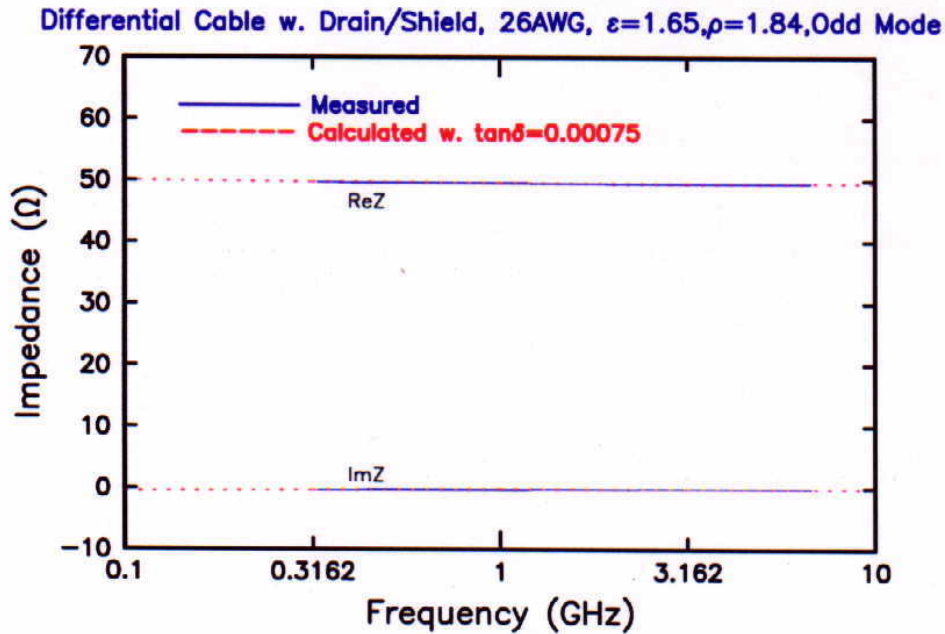


Fig. 9. Measured (solid) and calculated (dashed) complex impedance (ReZ_o and ImZ_o) for the AWG26 cables of Fig. 1 and for odd-mode, + -, differential excitation.

Diff.Cables,Braided Gnd 24AWG,Drain Gnd 26AWG,R =.001244/.001348ohm/cm

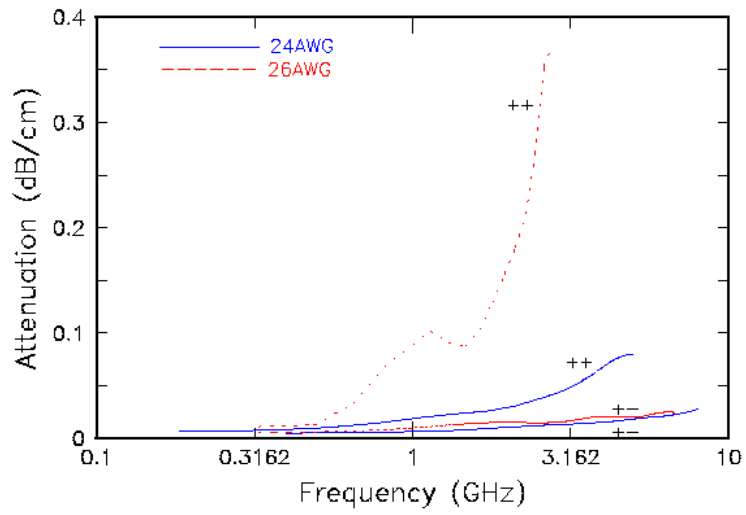


Fig. 10. Measured attenuations for the AWG26 (dashed) and AWG24 (solid) cables of Figs. 1 and 2 for odd-mode, + -, and even-mode, + +, differential excitations.

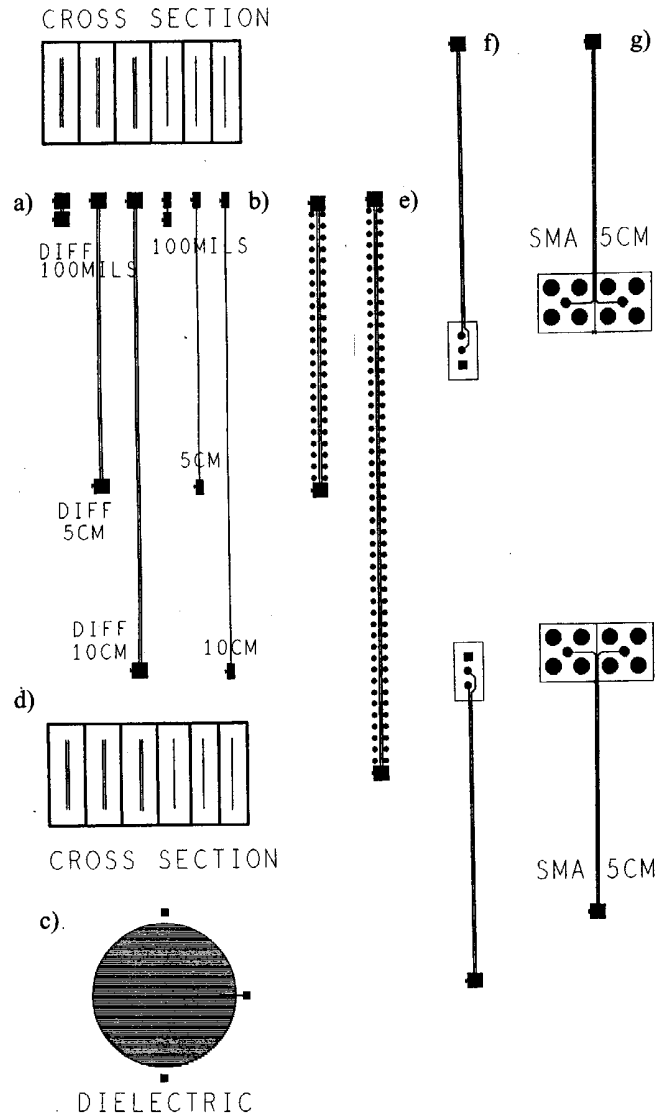


Fig. 11. Top view of the layout for the test card used for card wiring, with a) coupled lines, b) single lines, c) parallel-plate circular plate, d) cross sectioning sites, e) coupled lines with vias, f) 5-cm card connections to AWG24 cables having Quietzone connectors, and g) 5-cm differential card wiring connections to RG400 cables having SMA connectors.

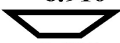

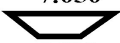

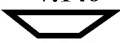


Coupled w/o Vias				Coupled w. Vias GS			
1.335				1.366			
6.910	10.59	6.910	11.91	7.050	10.45	7.050	11.90
			1.293				1.360
6.695		6.695	12.46	6.800		6.800	13.66
0.825				0.880			
Coupled w. Vias SSG				Single			
1.310				1.295			
7.140	10.36	7.140	12.00	6.805			12.01
			1.300				1.270
6.900		6.900	13.50	6.600			12.97
0.854				0.815			

Fig. 12. Cross sectional dimensions for the single wiring, coupled wiring, coupled wiring with GS, and coupled wiring with SSG vias having the layout shown in Fig. 11.

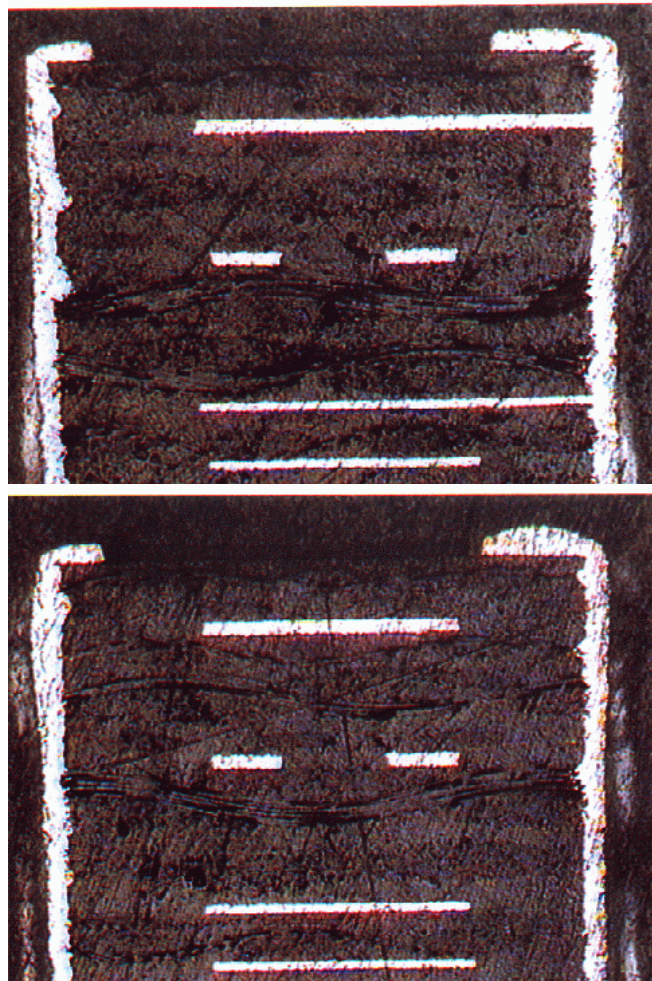


Fig. 13. Cross sections obtained for the coupled card wiring with GS and coupled wiring with SSG vias shown in Fig. 12.

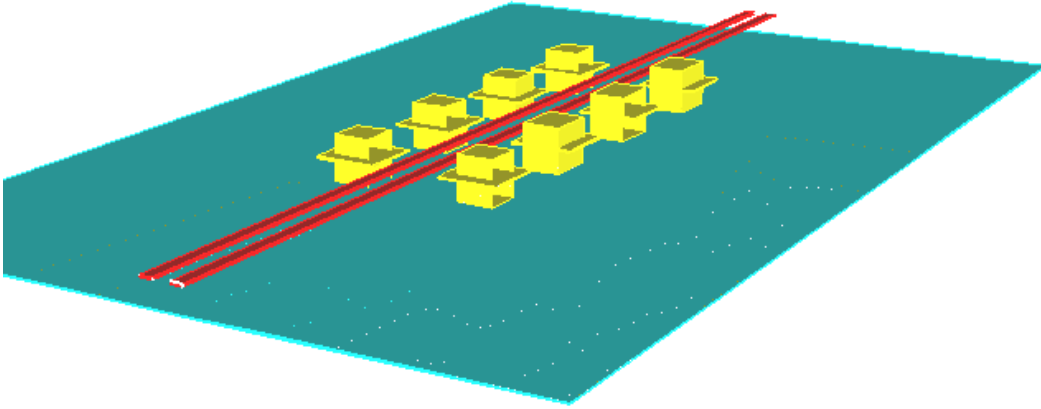
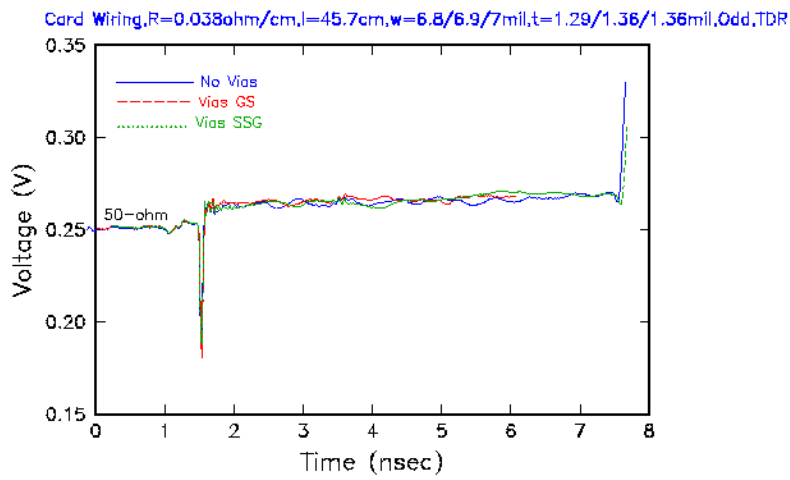


Fig. 14. Three-dimensional model of the coupled line card wiring with GS vias with the top ground plane removed for better viewing.

a)



b)

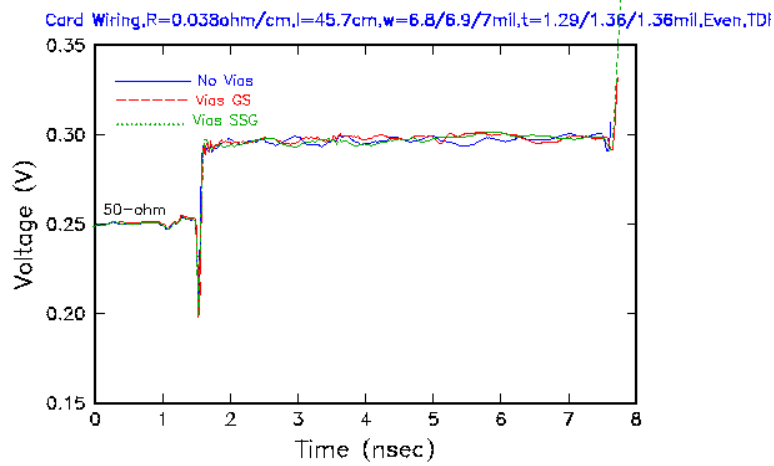


Fig. 15. TDR waveforms for the 45.7-cm-long differential card wiring using a) odd-mode and b) even-mode excitations, with 30-ps-step sources, and for the cases without vias (solid), with GS vias (dashed), and SSG vias (dotted) and the test card shown in Fig. 10.

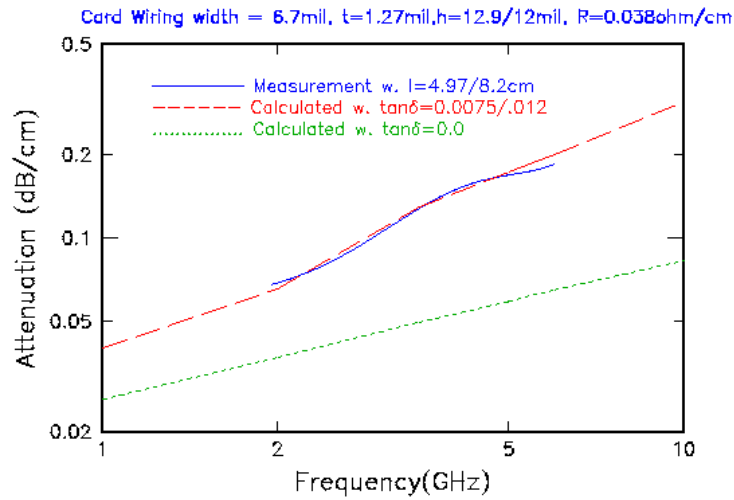


Fig. 16. Measured (solid) and calculated attenuation with $\tan\delta = 0.0$ (dotted) and $\tan\delta = 0.0075/0.012$ (dashed) for single line wiring using 4.97-cm and 8.2-cm lengths wiring and the short-pulse-propagation technique.

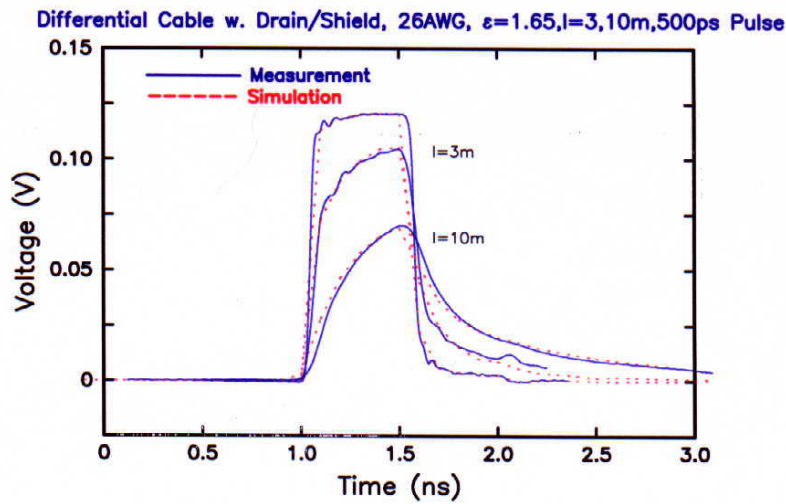


Fig. 17. Measured (solid) and simulated (dotted) pulse response for 500-ps input pulses for odd-mode excitation and 3-m- and 10-m-long AWG26 cables of the type shown in Fig. 1.

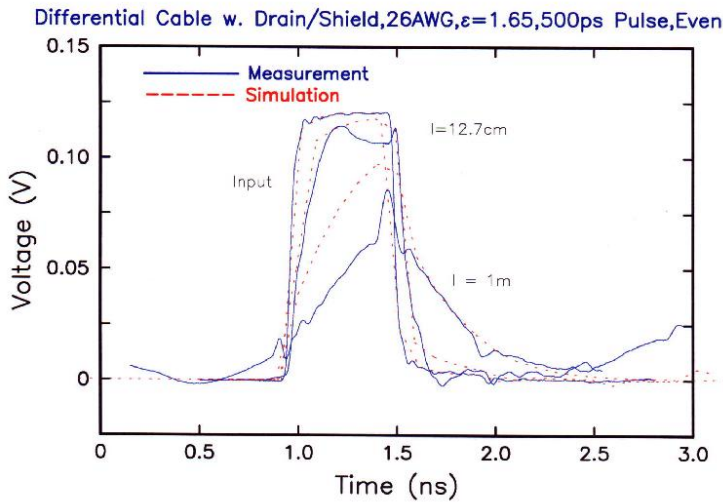


Fig. 18. Measured (solid) and simulated (dotted) pulse response for 500-ps input pulses for even-mode excitation and 12.7-cm- and 1-m-long AWG26 cables of the type shown in Fig. 1 and the test card shown in Figs. 4 and 5.

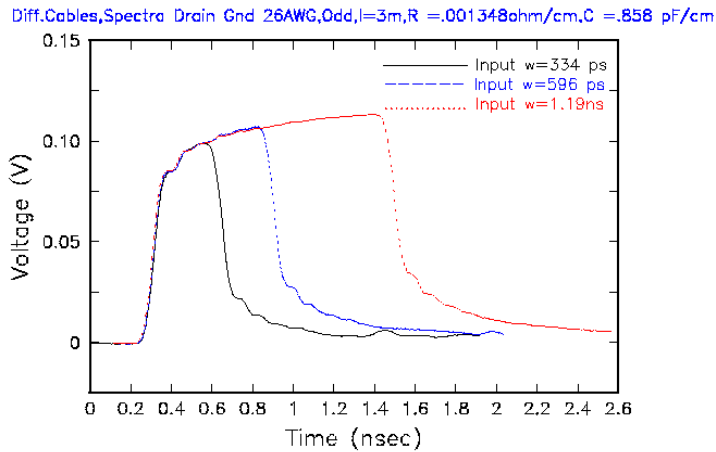


Fig. 19. Measured odd-mode excitation response for the AWG26 cables of Fig. 1 for 3-m lengths and 334-ps (solid), 596-ps (dashed), and 1.19-ns (dotted) wide pulses and using the test card shown in Figs. 4 and 5.

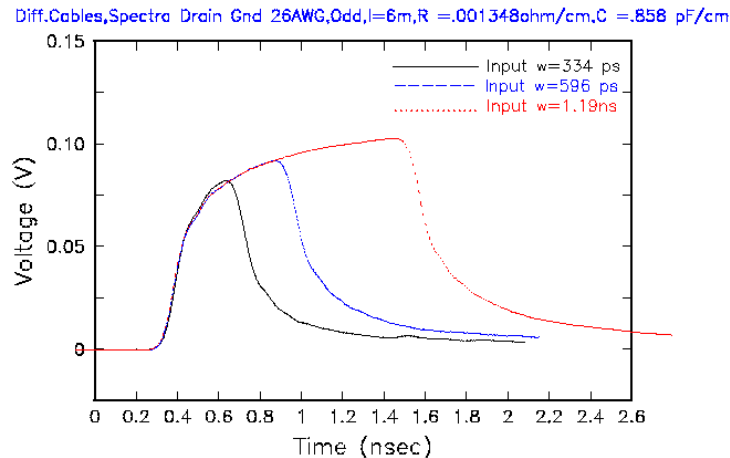


Fig. 20. Measured odd-mode excitation response for the AWG26 cables of Fig. 1 for 6-m lengths and 334-ps (solid), 596-ps (dashed), and 1.19-ns (dotted) wide pulses and using the test card shown in Figs. 4 and 5.

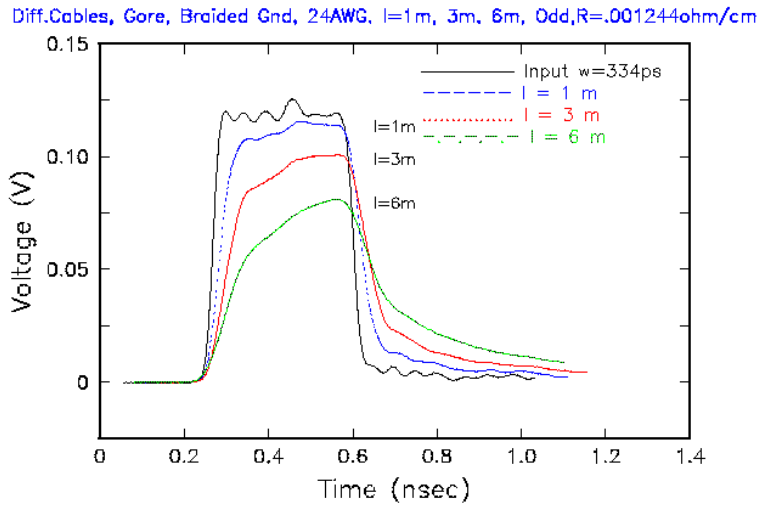


Fig. 21. Measured odd-mode excitation response for the AWG24 cables of Fig. 2 for 1-m (dashed), 3-m (dotted), and 6-m (dot-dashed) lengths and 334-ps (solid) wide pulse sources and using the test card shown in Figs. 4 and 5.

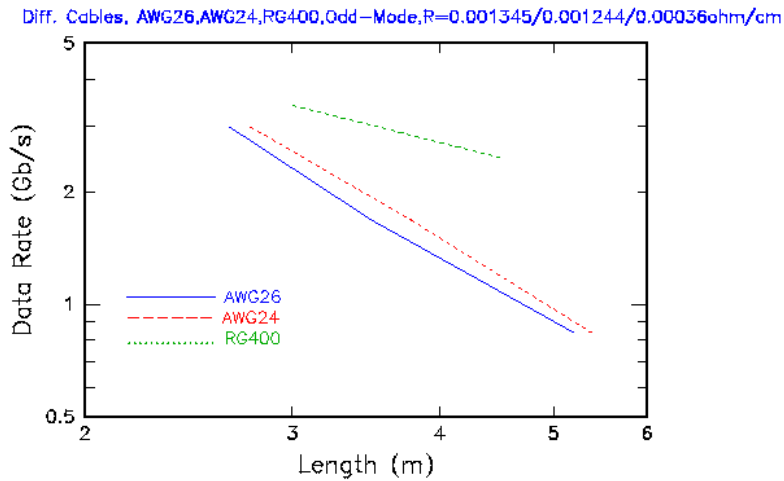


Fig. 22. Data rates for AWG26 (solid), AWG24 (dashed), and RG400 (dotted) cables based on measurements in odd-mode excitation and allowing the amplitude to degrade to 85% and the total loss to be 4.5 dB for the AWG26 cables, 3.5 dB for the AWG24 cables and 2.8-3.6 dB for the RG400 cables. In all cases, the results are for cables without connectors attached.

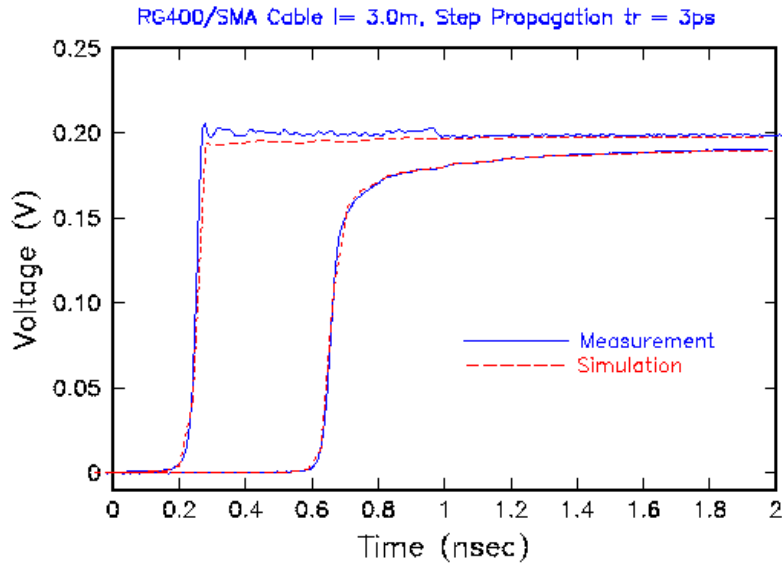


Fig. 23. Measured (solid) and simulated (dashed) TDT waveforms for the RG400 cables of Fig. 3 for 3-m length and 35-ps step excitation and using the test card shown in Fig. 4. The output waveforms are shifted in time to allow viewing.

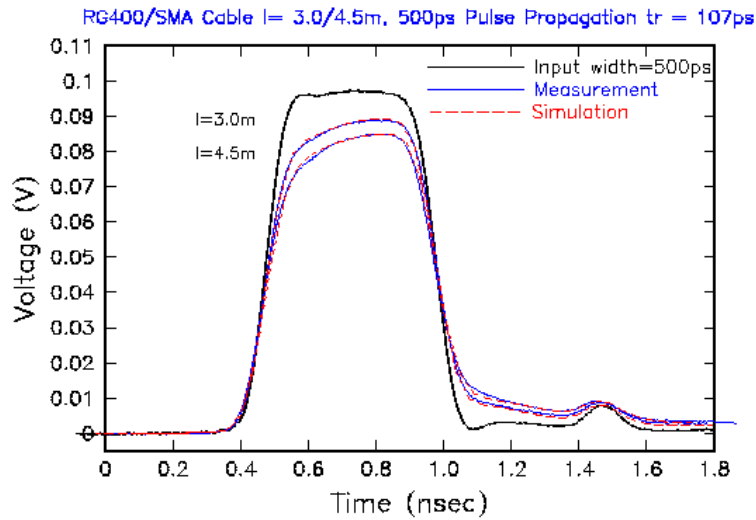


Fig. 24. Measured (solid) and simulated (dashed) pulse response for the RG400 cables with SMA connectors and using 500-ps wide pulse sources with 107-ps rise-time for 3-m and 4.5-m lengths.

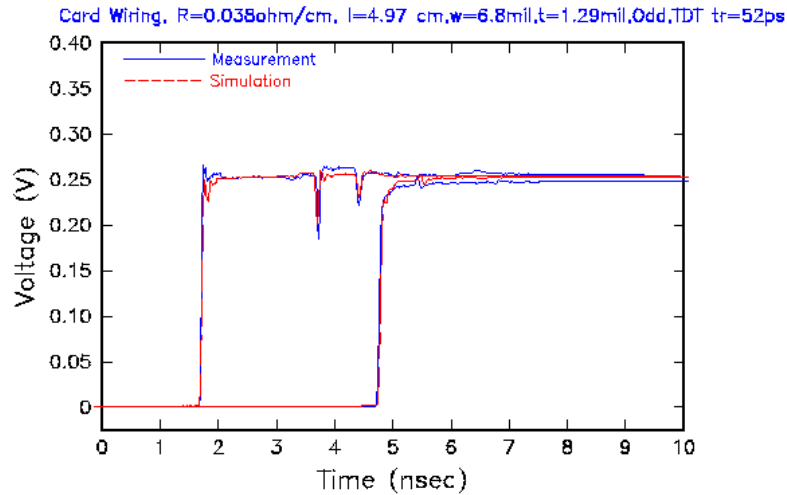


Fig. 25. Measured (solid) and simulated TDT waveforms (dashed) for 4.97-cm-long differential card wiring of the type shown in Fig. 12, using 52-ps rise-time sources in odd-mode excitation and with the test card layout shown in Fig. 11a.

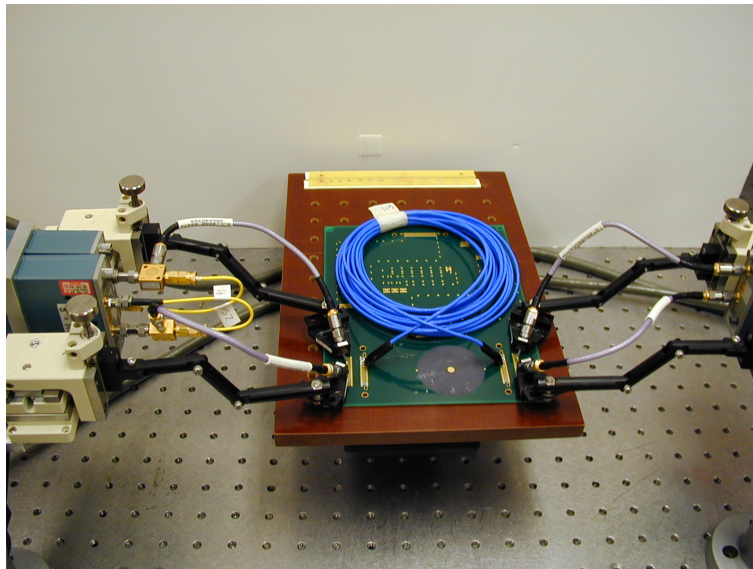


Fig. 26. Measurement set-up for testing the AWG24 cables with Quietzone connectors attached to 1.72-cm-long card wiring in strip-line configuration. Four Picoprobes are used for odd-mode excitation and pulse sources are generated with short coaxial cables and coaxial splitters attached to two Tektronix SD-24 and two SD-20 sampling heads.

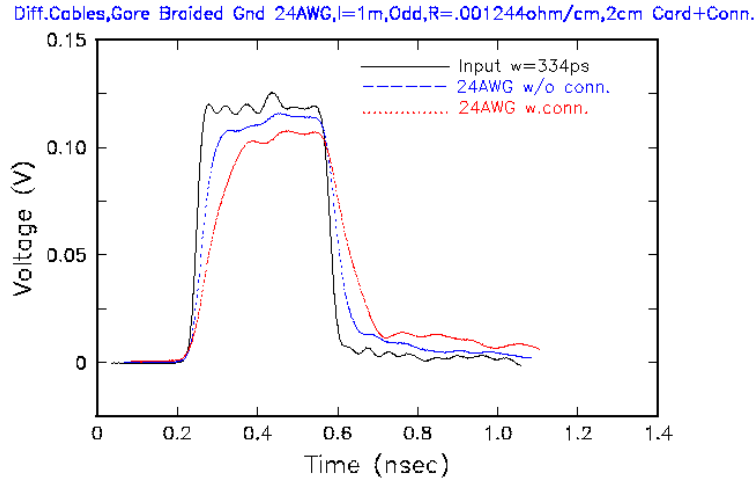


Fig. 27. Measured pulse response for 334-ps-wide input source (solid) in odd-mode excitation on 1-m-long AWG24 cables with the Quietzone connectors and card wiring in the path (dotted) as shown in Fig. 26 and without connectors (dashed). All pulses are shifted in time close to the source.

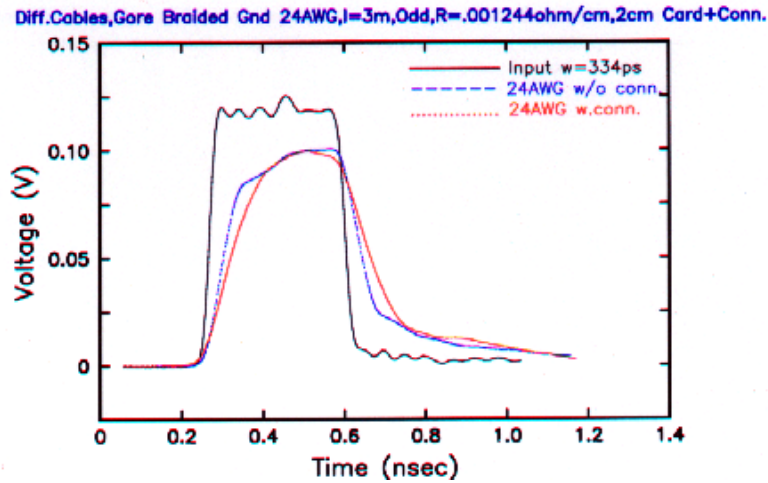


Fig. 28. Measured pulse response for 334-ps-wide input source (solid) in odd-mode excitation on 3-m-long AWG24 cables with the Quietzone connectors and card wiring in the path (dotted) as shown in Fig. 26 and without connectors (dashed). All pulses are shifted in time close to source.

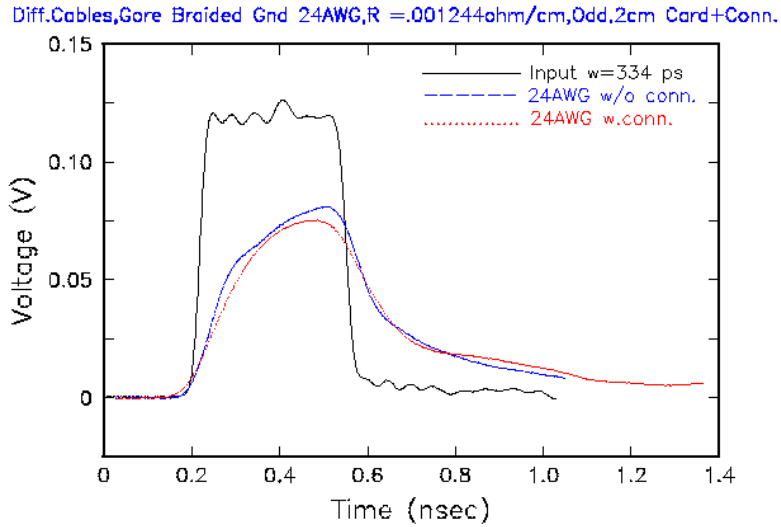


Fig. 29. Measured pulse response for 334-ps-wide input source (solid) in odd-mode excitation on 6-m-long AWG24 cables with the Quietzone connectors and card wiring in the path (dotted) as shown in Fig. 25 and without connectors (dashed). All pulses are shifted in time close to source.

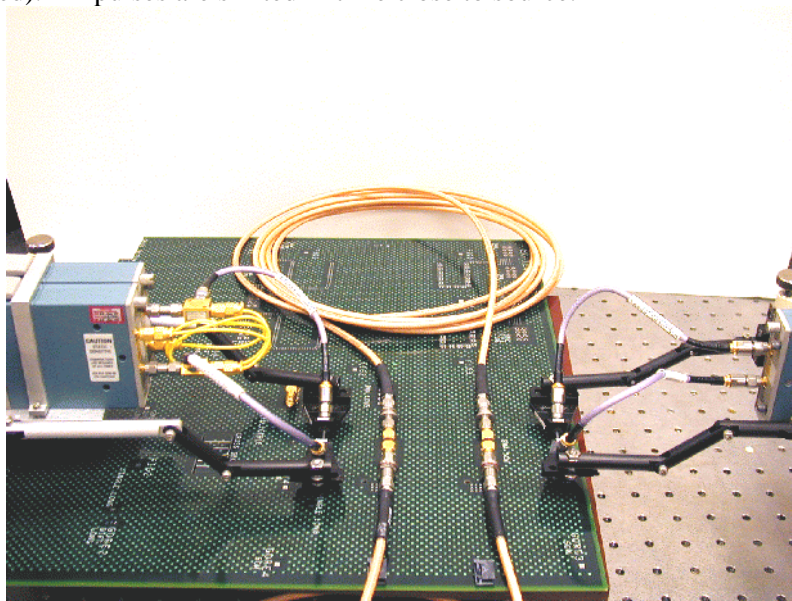


Fig. 30. Measurement set-up for testing the RG400 cables with SMA connectors and bulk-head adapters to 5-cm-long card wiring in strip-line configuration. Four Picoprobes are used for odd-mode excitation and pulse sources are generated with short coaxial cables and coaxial splitters attached to two Tektronix SD-24 and two SD-20 sampling heads. Two delay-matched cables are used for the differential pair.

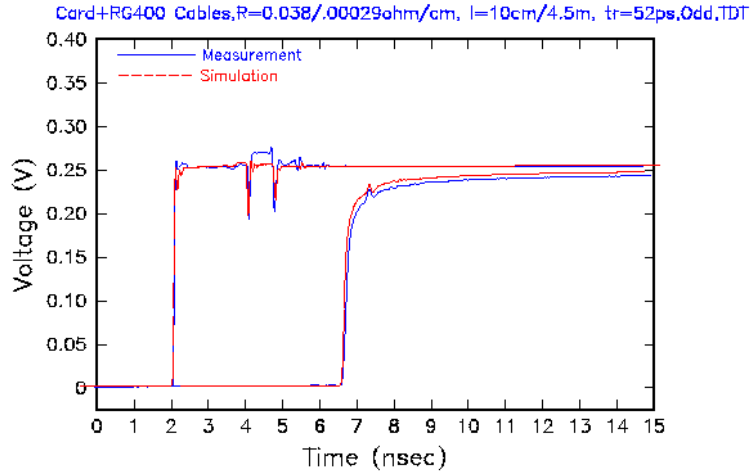


Fig. 31. Measured (solid) and simulated TDT waveforms (dashed) for two sections of 5-cm-long differential card wiring of the type shown in Fig. 11 and two 4.5-m-long RG400 cables, using 52-ps rise-time sources in odd-mode excitation and with the test card shown in Fig. 30.

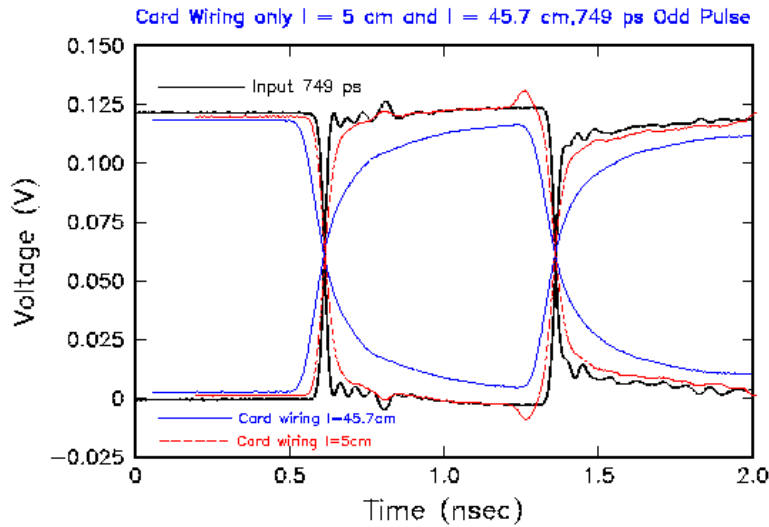


Fig. 32. Measured pulse response for 749-ps-wide input source (solid) in odd-mode excitation on 5-cm-long (solid) and 45.7-cm-long card wiring (dashed) of the type shown in Fig. 12. All waveforms are shifted close to input source.

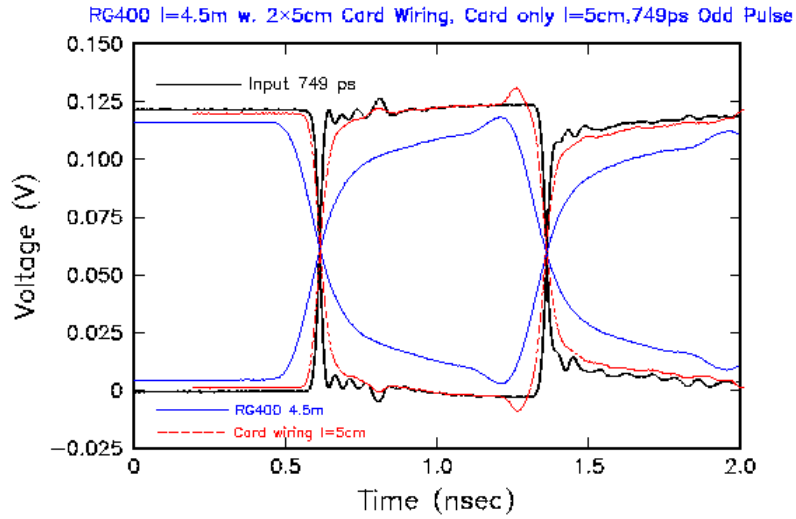


Fig. 33. Measured pulse response for 749-ps-wide input source (solid) in odd-mode excitation on 5-cm-long (solid) card wiring (dashed) of the type shown in Fig. 12 and 4.5-m-long RG400 cables. All waveforms are shifted close to input source.

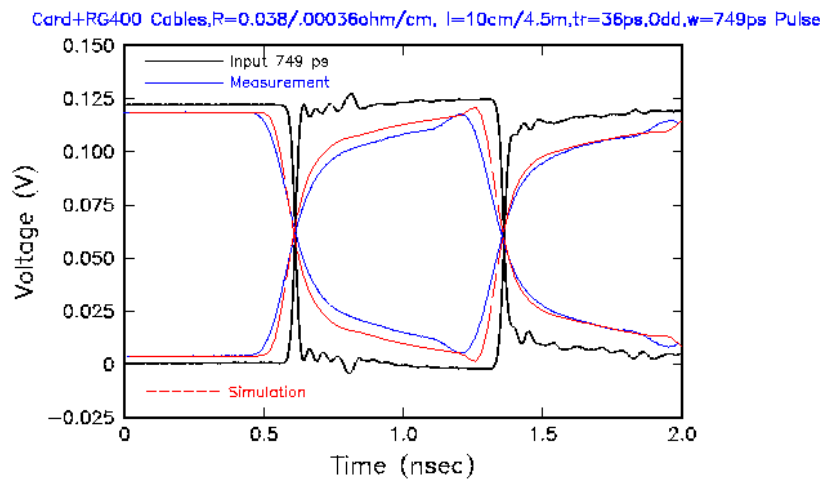


Fig. 34. Measured (solid) and simulated (dashed) pulse response for 749-ps-wide input source (solid) in odd-mode excitation on two sections of 5-cm-long card wiring of the type shown in Fig. 12 and 4.5-m-long RG400 cables with the test card shown in Fig. 30. All waveforms are shifted close to input source.

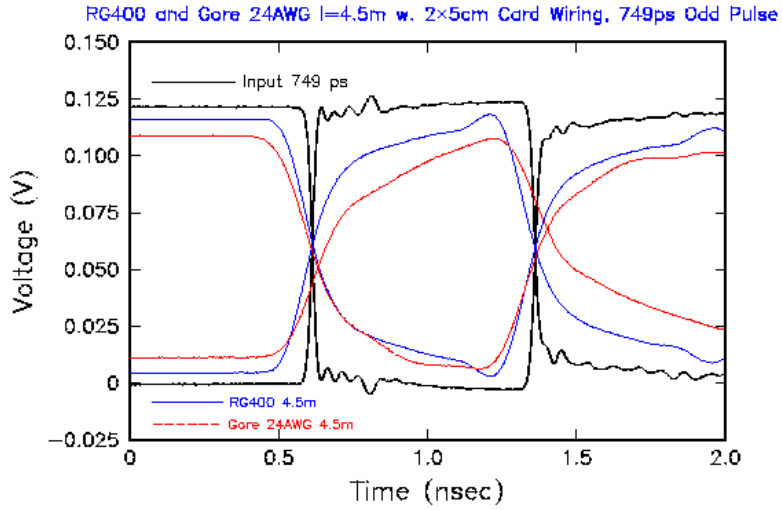


Fig. 35. Measured pulse response for 749-ps-wide input source (solid) in odd-mode excitation on two sections of 5-cm-long card wiring and 4.5-m-long RG400 cables (solid) with the card layout shown in Fig. 11g and 4.5-m-long AWG24 cables with the layout of Fig. 11f. All waveforms are shifted close to input source.

Table I. Measured cable and card wiring attenuations.

	AWG26	AWG24	RG400	Card
Freq.	Measured Attenuation			
(GHz)	(dB/cm)			
0.316	0.0054	0.0045	0.0024	0.0188
1.000	0.0100	0.0065	0.0043	0.0400
3.162	0.0167	0.0137	0.0080	0.1226
5.000	0.0204	0.0185	0.0103	0.1725
6.750	0.0249	0.0227	-----	0.2120
7.990	-----	0.0279	-----	-----
10.00	-----	-----	0.0212	-----

Table II. Measured and Calculated Card Wiring

Single Line Capacitance		
Calculated (pF/cm)	Δ	Measured (pF/cm)
1.1699	+3.4%	1.1315

Coupled-Line Capacitance		
Calculated (pF/cm)	Δ	Measured (pF/cm)
C11 1.2170	+5.9%	1.1490
C12 0.1593	+3.0%	0.1545

Table III. Measured and calculated characteristic impedance.

Pulse	Calc.	TDR	Pulse	Calc.	TDR
Odd-Mode			Even-Mode		
	Δ	Δ	l = 5 cm	Δ	Δ
54.3 Ω	50.1 Ω	54.3 Ω	67.2 Ω	65.2 Ω	69 Ω
	-7.7%	0		-3%	+2.7%
l = 5 cm with GS vias					
50.8 Ω	49.4 Ω	55.5 Ω	69.8 Ω	65.6 Ω	71.7 Ω
	-2.8%	+9.3%		-6%	+2.7%
l = 5 cm with SSG vias					
48.9 Ω	49.5 Ω	56.5 Ω	-----	65.7 Ω	72.2 Ω
	+1.2%	+15.5%			
l = 45 cm					
-----	50.1 Ω	55.0 Ω	-----	65.2 Ω	73.2 Ω
l = 45 cm with GS vias					
-----	49.4 Ω	56.2 Ω	-----	65.6 Ω	73.5 Ω
l = 45 cm with SSG vias					
-----	49.5 Ω	56.0 Ω	-----	65.7 Ω	72.9 Ω
l = 5 cm Single Line					
58.9 Ω	58.9 Ω	63.3 Ω			
	0	+7.5%			

Table IV. Differential Cable Pulse Measurements

334ps Pulse			596ps Pulse		1.19ns Pulse	
Length (m)	AWG24	AWG26	Signal Amplitude		AWG24	AWG26
	(%)	(%)	AWG24	AWG26		
0	100	100	100	100	100	100
1	97.5	96.6	96.0	96.0	96.7	98.4
3	84.0	83.0	87.0	87.8	91.8	91.8
4	-----	80.6	-----	82.0	-----	89.4
6	68.0	69.0	74.8	74.8	83.7	82.9
Length (m)	AWG24	AWG26	Pulse Width		AWG24	AWG26
	(%)	(%)	AWG24	AWG26		
0	100	100	100	100	100	100
1	97.7	96.6	98.7	99.3	100	100
3	90.4	89.8	97.3	97.3	100	99.0
4	-----	87.6	-----	95.3	-----	99.0
6	70.6	73.4	83.2	83.9	94.0	94.0
Length (m)	AWG24	AWG26	Risetime 40-60%		AWG24	AWG26
	(ps)	(ps)	AWG24	AWG26		
0	6	6	6	6	6	6
1	12	16	16	12	16	16
3	26	24	28	28	30	30
4	-----	36	-----	44	-----	40
6	130	112	140	136	140	150

Table V. 749-ps-wide pulse propagation on full path.

	Swing(mV)	Risetime(ps)	Δt
Input	124.0	36	9
5-cm Card	122.0	122	14.4
5-cm Card w. GS vias	122.0	123	16.6
45.7-cm Card	113.7	262	37.4
45.7-cm Card w. GS vias	113.7	267	37.4
4.5m-RG400 Cable w. 10-cm Card	113.9	254	49.2
4.5m-AWG24 Cable w. 10-cm Card	96.2	324	55.2
4.5m-RG400 Cable w. 10-cm Card, w/o bulkhead adapt.	113.9	258	45.6
4.5m-RG400 Cable w. 90° SMA/bulkhead adapt.	113.4	206	19.2

